Relativistic self-energy in nuclear dynamics

O. Plohl and C. Fuchs

Institut für Theoretische Physik, Universität Tübingen, Auf der Morgenstelle 14, D-72076 Tübingen, Germany
(Received 15 May 2006; published 22 September 2006)

It is a well-known fact that Dirac phenomenology of nuclear forces predicts the existence of large scalar and vector mean fields in matter. To analyze the relativistic self-energy in a model independent way, modern high-precision nucleon-nucleon (*NN*) potentials are mapped on a relativistic operator basis using projection techniques. Comparison of the various potentials at the level of covariant amplitudes produced remarkable agreement. It allows further calculation of the relativistic self-energy in nuclear matter in the Hartree-Fock approximation. Independent of the choice of the nucleon-nucleon interaction large scalar and vector mean fields of several hundred MeV magnitude are generated at tree level. In the framework of chiral effective field theory, these fields are dominantly generated by contact terms that occur at next-to-leading order in the chiral expansion. Consistent with Dirac phenomenology the corresponding low-energy constants that generate the large fields are closely connected to the spin-orbit interaction in *NN* scattering. The connection to quantum chromodynamics sum rules is discussed as well.

I. INTRODUCTION

A fundamental question in nuclear physics is the role relativity plays in nuclear systems. The ratio of the Fermi momentum over the nucleon mass is about $k_F/M \simeq 0.25$ and nucleons move maximally about 1/4 the velocity of light. This implies only moderate corrections from relativistic kinematics in finite nuclei. Nonrelativistic approaches such as, e.g., Skyrme-Hartree-Fock and relativistic approaches, describe finite nuclei equally well.

However, there exists a fundamental difference between relativistic and nonrelativistic dynamics: a genuine feature of relativistic nuclear dynamics is the appearance of large scalar and vector mean fields, each of a magnitude of several hundred MeV. The scalar field Σ_s is attractive and the vector field Σ_μ is repulsive. In relativistic mean-field (RMF) theory, both the sign and the size of the large scalar and vector fields are enforced by the nuclear saturation mechanism [1]. At nuclear saturation density $\rho_0 \simeq 0.16 \, \text{fm}^{-3}$ the empirical fields deduced from RMF fits to finite nuclei are of the order of $\Sigma_s \simeq -350$ MeV and $\Sigma_0 \simeq +300$ MeV [2] (in mean-field theory only the timelike component of Σ_μ contributes in static systems with time-reversal symmetry).

A problem is, however, that these scalar/vector fields are no direct observables as, e.g., the nuclear binding energy or the nucleon potential. The single-particle potential in which the nucleons move originates from the cancelation of the two contributions $U_{\text{cent}} \simeq \Sigma_0 + \Sigma_s$ and is of the order of -50 MeV. Therefore one has no direct experimental access to the interpolating scalar/vector fields. There exist, however, several features in nuclear structure that can be explained naturally within Dirac phenomenology, whereas models based on nonrelativistic dynamics have difficulties or, at least, one has to introduce additional model parameters. The most well-known feature is the large *spin-orbit splitting* in finite nuclei. In a relativistic framework the strong spin-orbit force appears naturally from the coupling to the lower components of the Dirac equation where the scalar-vector mean fields add up in

the spin-orbit potential $U_{\text{S.O.}} \propto (\Sigma_0 - \Sigma_s) \simeq 750$ MeV. Due to this fact RMF theory is able to reproduce the strong spin-orbit splitting in spherical nuclei quantitatively without the introduction of additional parameters [2]. A second symmetry, observed more than 30 years ago in single-particle levels of spherical nuclei is the so-called *pseudospin symmetry* [3]. Although all attempts to understand this symmetry within nonrelativistic approaches failed, it can naturally be understood within RMF theory as has been shown by Ginocchio [4] a few years ago. This symmetry, again a consequence of the coupling to the lower components, is exact in the limit $\Sigma_0 = -\Sigma_s$ and is broken in nature by the amount $(\Sigma_0 + \Sigma_s)/(\Sigma_0 - \Sigma_s)$ that is less than 10%. A third example are the *moments of inertia in rotating nuclei*. Relativistic dynamics implies that in the rotating system a Coriolis term occurs due to the spatial vector currents, however, with all couplings already fixed through the timelike components [5].

An alternative approach for nuclear matter are *ab initio* many-body calculations. Based on high precision nucleon-nucleon (*NN*) interactions one treats short-range and many-body correlations explicitly. A typical example for a successful many-body approach is Brueckner theory [10]. In the relativistic Brueckner approach the nucleon inside the medium is dressed by the self-energy Σ. The in-medium T matrix is obtained from the relativistic Bethe-Salpeter (BS) equation and plays the role of an effective two-body interaction that contains all short-range and many-body correlations of the ladder approximation. Solving the BS equation the Pauli principle is respected and intermediate scattering states are projected out of the Fermi sea. The summation of the T-matrix over the occupied states inside the Fermi sea yields finally the self-energy in Hartree-Fock approximation [11–15,47]. In contrast to relativistic Dirac-Brueckner-Hartree-Fock (DBHF) calculations that came up in the late 1980s nonrelativistic BHF theory has already half a century's history [10]. Despite strong efforts invested in the development of improved solution techniques for the Bethe-Goldstone (BG) equation,

the nonrelativistic counterpart of the BS equation, it turned out that, although such calculations were able to describe the nuclear saturation mechanism qualitatively, they failed quantitatively. Systematic studies for a large number of nucleon-nucleon interactions showed that saturation points were always allocated on a so-called *Coester-line* in the $E/A - \rho$ plane that does not meet the empirical region of saturation. In particular modern one-boson-exchange (OBE) potentials lead to strong overbinding and to too large saturation densities where relativistic calculations work much better [13,16].

However, in relativistic approaches the nuclear interaction is always described in some sort of a meson exchange picture. The mesons represent effective bosonic degrees of freedom that are either directly adjusted to the properties of nuclear matter and finite nuclei, as in the case of RMF theory, or to vacuum *NN* scattering. Hence, it is a fundamental question to decide whether the large scalar and vector fields enforced by Dirac phenomenology of nuclear systems are an artifact of the meson exchange picture or whether they reflect a deeper characteristics of nature.

A connection to quantum chromodynamics (QCD) as the fundamental theory of strong interactions is established by QCD sum rules [6,7]. The change of the chiral condensates $\langle \bar{q}q \rangle$, $\langle q^\dagger q \rangle$ in matter leads to attractive scalar and repulsive vector self-energies that are astonishingly close to the empirical values derived from RMF fits to the nuclear chart.

It is remarkable that relativistic many-body calculations again yield scalar and vector fields that are of the same sign and magnitude as obtained from RMF theory or, alternatively, from QCD sum rules. Such a coincidence could not have been expected *a priori*. Moreover, DBHF calculations [14] agree even on a quantitative level surprisingly well with the QCD-based approach of Ref. [9], where chiral fluctuations from the long and intermediate range pion-nucleon dynamics were considered on top of the chiral condensates.

These facts suggest that preconditions for the existence of large fields in matter or, alternatively, the density dependence of the QCD condensates, must already be inherent in the vacuum *NN* interaction. The connection of the nucleon-nucleon force to QCD is given by the fact that the interaction is described by the exchange of the low-lying mesonic degrees of freedom. The long-range part of the interaction is mediated by one-pion exchange (OPE), whereas the scalar isoscalar intermediate range attraction is mainly due to correlated two-pion-exchange. The short-range part, i.e., the hard core, is dominated by light vector meson exchange, i.e., the vector isoscalar ω meson and the vector isovector ρ. Modern one-boson-exchange potentials (OBEP) as, e.g., the Bonn potentials [17] are based on the exchange of these mesons and provide high-precision fits to nucleon-nucleon scattering data. Meson-nucleon coupling constants and form factors are empirically fixed from the data. Thus OBEPs are the result of relativistic phenomenology at the level of the elementary *NN* interaction. However, there also high-precision nonrelativistic empirical potentials such as the Argonne potential [18] or the Nijmegen potentials [20].

A more systematic and direct connection to QCD is provided by chiral effective field theory (EFT). Up to now

the two-nucleon system has been considered at next-to-next-to-next-to-leading order (N³LO) in chiral perturbation theory [22–24]. In such approaches the *NN* potential consists of one-, two-, and three-pion exchanges and contact interactions that account for the short-range contributions. The advantage of such approaches is the systematic expansion of the *NN* interaction in terms of chiral power counting. The expansion is performed in powers of $(Q/\Lambda_\chi)^\nu$, where Q is the generic low momentum scale given by the nucleon three-momentum or the four-momenta of virtual pions or a pion mass. $\Lambda_\chi \simeq 4\pi f_\pi \simeq 1$ GeV is the chiral symmetry breaking scale that coincides roughly with the Borel mass Λ_B of the sum rules. In such an expansion the low-energy constants (LECs) related to pion-nucleon vertices can be fixed from pion-nucleon scattering data [24].

A better understanding of the common features and the differences of the various approaches is essential to arrive at a more model independent understanding of the *NN* interaction, in particular since all the well established interactions fit *NN*-scattering data with approximately the same precision. A direct comparison of relativistic phenomenology based on the meson exchange picture with chiral EFT and nonrelativistic phenomenology is, however, difficult because the latter two approaches lack of a clear Lorentz structure. At low-momentum scales the different potentials can be mapped on each other using renormalization group methods [25]. This led recently to the construction of a "model independent" low-momentum potential $V_{\mathrm{low}\,k}$ by integrating out the dynamics for momenta above a cutoff scale of about $\Lambda \simeq 2\,\mathrm{fm}^{-1}$ [25]. It has been argued that beyond this scale the short-range part of the interaction, mediated by vector meson exchange or pointlike counter terms, becomes dominant and leads to the deviations of the various approaches.

Although a breakthrough in some sense, the renormalization group approach does not help to clarify the relativistic structure of the potentials which is essential, e.g., to generate (or not to generate) large scalar/vector mean fields in nuclear matter.

The present work tries to answer this question. We apply projection techniques to map the various potentials on Dirac phenomenology. The philosophy behind this approach is based on the fact that any *NN* interaction, independent whether relativistic or nonrelativistic, contains a certain spin-isospin operator structure. By projection techniques this operator basis is mapped on the operator basis of Dirac phenomenology that is given by the Clifford algebra in Dirac space. This allows identification of the different Lorentz components of the interaction. Starting from the angular-momentum representation of a given *NN* potential, one transforms to plane-wave helicity states and finally to Lorentz invariant amplitudes in Dirac space [26,27]. Such a transformation is well defined in the positive energy sector for on-shell amplitudes and allows comparison of the *NN* potentials on the basis of Lorentz invariant amplitudes. A remarkable agreement among relativistic and nonrelativistic OBE potentials, nonrelativistic phenomenological potentials, and EFT potentials, respectively, was found in Ref. [46]. This agreement is also reflected in the structure of the relativistic self-energy when we further calculate the mean field in infinite nuclear matter in Hartree-Fock approximation at tree level. The

scalar and vector self-energy components are found to be large, i.e., of the order of several hundred MeV [46]. The present work extends the investigations of Ref. [46]. The formalism is outlined in detail and we discuss the density dependence of the fields as well as the implications for the nuclear equation of state. The connection between chiral EFT and QCD sum rules is investigated. The present formalism allows a quantitative extraction of the scalar/vector fields that are generated by pion dynamics and contact terms at different orders in the chiral expansion.

The article is organized as follows: in Sec. II we discuss the operator structure of the various potentials. The transformation onto the covariant basis is outlined in Sec. III, where the results of this analysis namely the Lorentz invariant amplitudes are also shown. Section IV contains the determination of the relativistic mean fields in nuclear matter. In Sec. V the structure of the relativistic self-energy fields from chiral EFT is discussed, as well as the connection to QCD sum-rule predictions. Finally the self-consistent Hartree-Fock results for the equation of state calculated with three different potentials (Bonn A, Nijm93, and Nijm I) are discussed in Sec. VI.

II. OPERATOR STRUCTURE OF THE NN POTENTIALS

A. OBE potentials

As typical examples for modern high-precision OBEPs we consider the Bonn A [37] and the high-precision, charge-dependent Bonn potential (CD-Bonn) [28]. The Bonn potentials are based on the exchange of the six nonstrange bosons $(\pi, \eta, \rho, \omega, \delta, \sigma)$ with masses below 1 GeV. These are the two scalar mesons σ (isoscalar) and δ (isovector), the two pseudoscalar mesons π (isovector) and η (isoscalar), and the two vector mesons ω (isoscalar) and ρ (isovector). The potentials are derived in the *no sea* approximation that neglects the coupling to antiparticles.

The Born scattering matrix is given by the sum over the corresponding scalar, pseudoscalar, and vector mesons and has the following structure

$$\hat{V}(q', q) = \sum_{\alpha=s, ps, v} \mathcal{F}_\alpha^2(q', q) \kappa_\alpha^{(2)} D_\alpha(q' - q) \kappa_\alpha^{(1)}. \quad (1)$$

In the two-nucleon center-of-mass frame (c.m.) the four-momenta of the incoming nucleons are $q_\mu^{(1/2)} = [E(\mathbf{q}), \pm\mathbf{q}]$ and correspondingly, the four-momenta of the outgoing nucleons are $q_\mu'^{(1/2)} = [E(\mathbf{q}'), \pm\mathbf{q}']$. The initial and final relative c.m. momenta are $q_\mu = \frac{1}{2}(q_\mu^{(1)} - q_\mu^{(2)})$ and $q_\mu' = \frac{1}{2}(q_\mu'^{(1)} - q_\mu'^{(2)})$, respectively. For on-shell scattering $|\mathbf{q}| = |\mathbf{q}'|$ with $E(\mathbf{q}) = E(\mathbf{q}') = \sqrt{M^2 + \mathbf{q}^2}$ the energy-transfer is zero, i.e., $q_\mu' - q_\mu = (0, \mathbf{q}' - \mathbf{q})$. The matrices (1) factorize for each meson α into the form factors $\mathcal{F}_\alpha$ at each meson-nucleon vertex, the meson propagator D_α, and the meson-nucleon vertices κ_α themselves. In the standard Bonn potentials [37] the phenomenological form factors have the form

$$\mathcal{F}_\alpha(q', q) = \left[\frac{\Lambda_\alpha^2 - m_\alpha^2}{\Lambda_\alpha^2 + (\mathbf{q}' - \mathbf{q})^2}\right]^{n_\alpha}, \quad (2)$$

where m_α is the corresponding meson mass and Λ_α is a cutoff to avoid divergences at short distances. The meson propagators read

$$D_{s, ps}(q' - q) = i \frac{1}{(q' - q)^2 - m_{s, ps}^2},$$

$$D_v^{\mu\nu}(q' - q) = i \frac{-g^{\mu\nu} + (q' - q)^\mu (q' - q)^\nu / m_v^2}{(q' - q)^2 - m_v^2}$$

(3)

for scalar and pseudoscalar mesons s, ps, and vector mesons v. The Dirac structure of the potential is contained in the meson-nucleon vertices

$$\kappa_s = \frac{g_s}{(2\pi)^2}\mathbf{1}, \quad \kappa_{ps} = \frac{g_{ps}}{(2\pi)^2} \frac{\slashed{q}' - \slashed{q}}{2M} i\gamma^5,$$

$$\kappa_v = \frac{1}{(2\pi)^2}\left(g_v \gamma^\mu + \frac{f_v}{2M} i\sigma^{\mu\nu}\right).$$

(4)

For the pseudoscalar mesons π and η a pseudovector coupling is used to fulfill soft pion theorems. The vertices of the isovector bosons π, δ, ρ obtain additional $\tau_2 \cdot \tau_1$ isospin matrices that are suppressed in Eqs. (4). The ω meson has no tensor coupling, i.e., $f_v^{(\omega)} = 0$.

The potential, i.e., the OBE Feynman amplitudes are obtained by sandwiching $\hat{V}$ between the incoming and outgoing Dirac spinors

$$V(\mathbf{q}', \mathbf{q}) = \sum_{\alpha=s, ps, v} \mathcal{F}_\alpha^2(\mathbf{q}', \mathbf{q}) D_\alpha(\mathbf{q}' - \mathbf{q})$$

$$\times \bar{u}_2(-\mathbf{q}') \kappa_\alpha^{(2)} u_2(-\mathbf{q}) \bar{u}_1(\mathbf{q}') \kappa_\alpha^{(1)} u_1(\mathbf{q}). \quad (5)$$

The relativistic operator structure is thus completely determined by the matrix elements of the vertices κ_α. In helicity representation the Dirac spinor basis is given by

$$u_\lambda(\mathbf{q}) = \sqrt{\frac{E + M}{2M}}\left(\begin{array}{c} 1 \\ \frac{2\lambda|\mathbf{q}|}{E+M} \end{array}\right)\chi_\lambda, \quad (6)$$

where χ_λ denotes a two-component Pauli spinor with $\lambda = \pm\frac{1}{2}$. The normalization of the Dirac spinor is chosen such that $\bar{u}_\lambda u_\lambda = 1$.

A consequence of the Feynman amplitudes (5) is their general nonlocal structure that distinguishes the field theoretical relativistic OBE approach from local nonrelativistic potentials. This is even true for the relativistic OPE compared to the local, nonrelativistic OPE (see, e.g., the discussion in Ref. [29]). However, for on-shell scattering the relativistic amplitudes acquire a local structure in the sense that they are functions of $\mathbf{q}^2$ and $\mathbf{q}' - \mathbf{q}$. In particular for forward and backward scattering, i.e., $\theta = 0, \pi$, the amplitudes are "local" functions of $\mathbf{q}^2$ and $\mathbf{q}$. The nonlocal structure of the relativistic amplitudes becomes evident when going off-shell, e.g., in the intermediate states in the Bethe-Salpeter equation [29,30].

The standard Bonn (A,B,C) potentials [37] contain 13 free parameters for coupling constants and cutoff masses and two additional parameters if one considers the masses of the scalar mesons as effective parameters. The matrix elements are calculated with the OBNNS code of R. Machleidt [31] when Bonn A is used and the corresponding CDBONN package of R. Machleidt when CD-Bonn is used.

In contrast to the standard Bonn potentials [37] the OPE part of the CD-Bonn potential [28] accounts for charge symmetry breaking in nn, pp, and np scattering due to the different pion masses m_{π^0} and $m_{\pi^\pm}$. The CD-Bonn potential can be referred to as a phenomenological NN potential, because by fine-tuning of the partial wave fits χ^2 per datum is minimized to 1.02, adding up to a total of 43 free parameters.

1. Nonrelativistic reduction

The OBE potentials as, e.g., the Bonn potentials can be reduced to a nonrelativistic representation by expanding the full field-theoretical OBE Feynman amplitudes into a set of spin and isospin operators

$$V = \sum_i [V_i + V_i' \, \boldsymbol{\tau}_1 \cdot \boldsymbol{\tau}_2] \, O_i. \tag{7}$$

The operators O_i obtained in this low-energy expansion, assuming identical particle scattering and charge independence, are defined as

$$
\begin{aligned}
O_1 &= 1, \\
O_2 &= \boldsymbol{\sigma}_1 \cdot \boldsymbol{\sigma}_2, \\
O_3 &= (\boldsymbol{\sigma}_1 \cdot \mathbf{k})(\boldsymbol{\sigma}_2 \cdot \mathbf{k}) \\
O_4 &= \tfrac{i}{2}(\boldsymbol{\sigma}_1 + \boldsymbol{\sigma}_2) \cdot \mathbf{n}, \\
O_5 &= (\boldsymbol{\sigma}_1 \cdot \mathbf{n})(\boldsymbol{\sigma}_2 \cdot \mathbf{n}),
\end{aligned}
\tag{8}
$$

where $\mathbf{k} = \mathbf{q}' - \mathbf{q}$, $\mathbf{n} = \mathbf{q} \times \mathbf{q}' \equiv \mathbf{P} \times \mathbf{k}$, and $\mathbf{P} = \frac{1}{2}(\mathbf{q} + \mathbf{q}')$ is the average momentum. The potential forms V_i are then functions of $\mathbf{k}$, $\mathbf{P}$, $\mathbf{n}$ and the energy. To perform a nonrelativistic reduction, usually the energy E is expanded in $\mathbf{k}^2$ and $\mathbf{P}^2$

$$E(\mathbf{q}) = \left(\frac{\mathbf{k}^2}{4} + \mathbf{P}^2 + M^2 \right)^{\frac{1}{2}} \simeq M + \frac{\mathbf{k}^2}{8M} + \frac{\mathbf{P}^2}{2M}. \tag{9}$$

and terms to leading order in $\mathbf{k}^2/M^2$ and $\mathbf{P}^2/M^2$ are taken into account. The meson propagators $D_\alpha(k^2)$ given in Eq. (3) are approximated by their static form $(-1)/(\mathbf{k}^2 + m^2)$. The equivalent to Eq. (7) in configuration space is given by

$$
\begin{aligned}
O_1 &= 1, \\
O_2 &= \boldsymbol{\sigma}_1 \cdot \boldsymbol{\sigma}_2, \\
O_3 &= S_{12} = 3(\boldsymbol{\sigma}_1 \cdot \hat{\mathbf{r}})(\boldsymbol{\sigma}_2 \cdot \hat{\mathbf{r}}) - \boldsymbol{\sigma}_1 \cdot \boldsymbol{\sigma}_2, \\
O_4 &= \mathbf{L} \cdot \mathbf{S}, \\
O_5 &= Q_{12} = \tfrac{1}{2}[(\boldsymbol{\sigma}_1 \cdot \mathbf{L})(\boldsymbol{\sigma}_2 \cdot \mathbf{L}) + (\boldsymbol{\sigma}_2 \cdot \mathbf{L})(\boldsymbol{\sigma}_1 \cdot \mathbf{L})].
\end{aligned}
\tag{10}
$$

These operators are the well-known central, spin-spin, tensor, spin-orbit, and quadratic spin-orbit operators, respectively. The total angular momentum is denoted by $\mathbf{L} = \mathbf{r} \times \mathbf{P}$ and the total spin $\mathbf{S} = \frac{1}{2}(\boldsymbol{\sigma}_1 + \boldsymbol{\sigma}_2)$.

B. Nonrelativistic potentials

1. Meson-theoretical potentials

We consider the modern Nijmegen soft-core potential Nijm93 [19] as the first example of a nonrelativistic

meson-theoretical potential. It is an updated version of the Nijm78 [21] potential, where the low-energy NN interaction is based on Regge-pole theory leading to the well-known OBE forces. The contributions considered in this model are the pseudoscalar mesons π, η, η', the vector mesons ρ, ϕ, ω, the scalar mesons δ, S^*, ϵ, and the Pomeron P and the $J = 0$ tensor contributions, all in all 13 free parameters. Because it is constructed from approximate OBE amplitudes it is based on the operator structure given in Eq. (8) plus an additional operator $O_6 = \frac{1}{2}(\boldsymbol{\sigma}_1 - \boldsymbol{\sigma}_2) \cdot \mathbf{L}$ accounting for charge independence breaking, which is new compared to the older version Nijm78. Exponential form factors are used. This potential gives a χ^2 per datum of 1.87, which is comparable to similar OBE potentials such as the standard Bonn potentials.

2. Phenomenological potentials

Another class of nonrelativistic NN potentials are the so-called high-quality potentials where $\chi^2/N_{\text{data}} \approx 1.0$. Here we study the Nijmegen potentials Nijm I, Nijm II, and Reid93 [19]. The Nijm I and Nijm II potentials are both based on the Nijm78 potential. In the Nijm I potential some nonlocal terms in the central force are kept, whereas in the Nijm II potential all nonlocal terms are removed. Although based on the meson-theoretical Nijm78 potential these potentials are often referred to as purely phenomenological models, because the parameters are adjusted separately in each partial wave leading to a total of 41 parameters. At very short distances, both potentials are regularized by an exponential form factor.

The Nijmegen soft-core Reid93 [19] potential is a phenomenological potential and is therefore based on a completely different approach. In the meson-theoretical Nijmegen potential Nijm93 the potential forms V_i are the same for all partial waves, whereas in the Reid93 potentials every partial wave is parametrized separately by a convenient choice of combinations of central, tensor, and spin-orbit functions (local Yukawas of multiples of the pion mass) and the related operators, i.e., the operators O_1 to O_4 from Eq. (10). It is regularised by a dipole form factor and has 50 phenomenological parameters giving all in all a $\chi^2/N_{\text{data}} = 1.03$. All the Nijmegen potentials contain the proper charge-dependent OPE accounting for charge symmetry breaking in nn, pp, and np scattering due to different pion masses m_{π^0}, $m_{\pi^\pm}$.

The same holds for the Argonne potential v_{18} [18], also an example for a widely used modern high-precision phenomenological NN potential. It is given by the sum of an electromagnetic (EM) part, the proper OPE, and a phenomenological intermediate- and short-range part unrestricted by a meson-theoretical picture:

$$V = V^{\text{EM}} + V^\pi + V^R. \tag{11}$$

The EM interaction is the same as that used in the Nijmegen partial-wave analysis. Short-range terms and finite-size effects are taken into account as well [18].

The strong interaction part $V^\pi + V^R$ can be written in a form such as that given in Eq. (7) in configuration space, where the Argonne v_{18} potential is not constructed by approximating the field-theoretical OBE amplitudes (except for the OPE) but

by assuming a very general two-body potential constrained by certain symmetries. The potential forms V_i parametrizing the intermediate and short-range part are mostly local Woods-Saxon functions.

The local two-body operators are the same charge independent ones used in the Argonne v_{14} potential

$$O_i = 1, \quad \sigma_1 \cdot \sigma_2, \quad S_{12}, \quad \mathbf{L} \cdot \mathbf{S}, \quad L^2, \quad L^2(\sigma_1 \cdot \sigma_2), \quad (\mathbf{L} \cdot \mathbf{S})^2. \quad (12)$$

Due to isovector exchange these operators have to be multiplied by the isospin matrices $\tau_1 \cdot \tau_2$ that than adds up to 14 operators. Additionally, four operators accounting for charge independence breaking are introduced

$$O_{i=15,18} = T_{12}, \quad (\sigma_1 \cdot \sigma_2)T_{12}, \quad S_{12}T_{12}, \quad (\tau_{z1} + \tau_{z2}), \quad (13)$$

where $T_{12} = 3\tau_{z1}\tau_{z2} - \tau_1 \cdot \tau_2$, is the isotensor operator, defined analogously to the spin tensor S_{12} operator.

Thus the operator structure is more general than that imposed by a nonrelativistic, local OBE picture, in particular for the intermediate and short distance part. In total, Argonne v_{18} contains 40 adjustable parameters and gives a χ^2 per datum of 1.09 for 4301 pp and np data in the range 0–350 MeV [18]. The code used to calculate the potential matrix elements of the Argonne v_{18} model in momentum space was provided by H. Muether and T. Frick.

C. Low-energy potentials

1. EFT potentials

Following the concept originally proposed by Weinberg [32] there has been substantial progress in recent time to derive quantitative NN potentials from chiral effective field theory. As already mentioned, the chiral expansion is performed in powers of $(Q/\Lambda_\chi)^\nu$, where $\nu = 0$ corresponds to leading order (LO), $\nu = 2$ to next-to-leading order (NLO), $\nu = 3$ to next-to-next-to-leading (N^{2}LO), and finally $\nu = 4$ to next-to-next-to-next-to-leading order (N^{3}LO). It turned out that for a quantitative description of NN-scattering data one has to go up to N^{3}LO [22–24] in the chiral expansion for the two-nucleon problem. N^{2}LO contributions were still found to be very large compared to NLO. This implies that 2π (and 3π) contributions have to be included up to order four. The effective chiral Lagrangian can be written as

$$\mathcal{L}_{\text{eff}} = \mathcal{L}_{\pi\pi}^{(2)} + \mathcal{L}_{\pi N}^{(1)} + \mathcal{L}_{\pi N}^{(2)} + \mathcal{L}_{\pi N}^{(3)} + \cdots, \quad (14)$$

where the superscript refers to the number of derivatives or pion mass insertions (chiral dimension) and the ellipsis stands for terms of chiral order four or higher. The corresponding chiral NN potential is then defined by

$$V(\mathbf{q}', \mathbf{q}) \equiv \left\{ \begin{matrix} \text{sum of irreducible} \\ \pi + 2\pi \text{ contributions} \end{matrix} \right\} + \text{contacts}. \quad (15)$$

The 2π exchange contributions to the NN interaction at order four have been derived by Kaiser [33]. Recently, quantitative NN potentials including contact terms at order four were derived by Entem and Machleidt, the so-called Idaho potential [22,23], and by Epelbaum, Glöckle, and Meissner [24].

For the present comparison we apply the Idaho potential [23]. The operator structure of the momentum-space

NN amplitude has the general form given in Eq. (7) with the operators O_i from Eq. (8). The potential forms V_i ($i = C, S, T, LS, \sigma L$) can be expressed as functions of $|(\mathbf{q}' - \mathbf{q})|$ and $|\mathbf{k}|$.

The Idaho potential is regularized by an exponential cutoff

$$V(\mathbf{q}', \mathbf{q}) \longmapsto V(\mathbf{q}', \mathbf{q}) \, e^{-(q'/\Lambda)^{2n}} \, e^{-(q/\Lambda)^{2n}}, \quad (16)$$

where $\Lambda = 0.5$ GeV in all partial waves. This does not affect the chiral order of the potential but introduces contributions beyond that order. The total number of free model parameters in the N^{3}LO potential is 29 [23].

For the evaluation of the matrix elements we applied the N^{3}LO program package provided by D. Entem and R. Machleidt.

2. Renormalization Group approach to NN interaction

Recently, another approach has been proposed to arrive at a better model-independent understanding of the NN interaction [25]. In this approach a low-momentum potential $V_{\text{low }k}$ is derived from a given realistic NN potential by separating the low-momentum part, i.e., by integrating out the high-momentum modes, and using renormalization group (RG) methods to evolve the NN potential models from the full Hilbert space to the low-momentum subspace. At a cutoff of $\Lambda = 2.1$ fm^{-1} all the various NN potential models were found to collapse to a model-independent effective interaction $V_{\text{low }k}$.

Because elastic NN-scattering data constrain the NN interaction only up to a momentum scale of about 400 MeV, which corresponds to the pion threshold, modern high-precision potentials differ essentially in the treatment of the short-range part, as depicted in Fig. 1. The philosophy behind the RG approach is to replace the unresolved short distance structure by something simpler, e.g., contact terms, without distorting low-energy observables.

III. TRANSFORMATION TO A COVARIANT OPERATOR BASIS

A. Covariant operators in Dirac space

Any two-body amplitude can be represented covariantly by Dirac operators and Lorentz-invariant amplitudes. A detailed discussion of the general structure of relativistic two-body
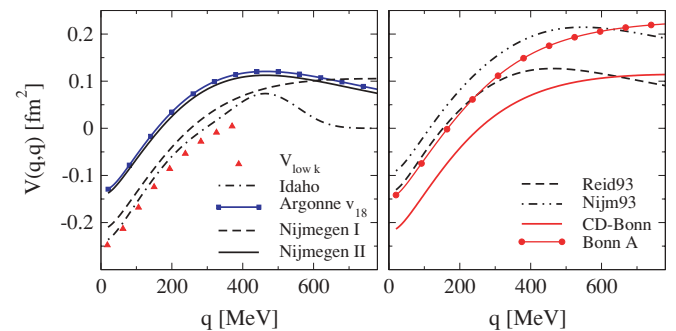

FIG. 1. (Color online) Diagonal matrix elements $V(\mathbf{q}, \mathbf{q})$ in the $^1S_0$ partial wave for different high-precision NN potential models.

amplitudes can be found in Refs. [26,34]. However, a relativistic treatment automatically invokes the excitation of antinucleons. Nucleon-nucleon scattering, in both the nonrelativistic approaches discussed above but also in the framework of the standard OBE potentials is restricted to the positive energy sector and neglects the coupling to antinucleons. As a consequence one has to work in a subspace of the full Dirac space that leads to on-shell ambiguities that require some care.

The inclusion of negative-energy excitations with 4 states for each spinor yields altogether $4^4 = 256$ types of two-body matrix elements with respect to their spinor structure. Symmetry arguments reduce these to 44 for on-shell particles [34]. If one takes only the subspace of positive energy solutions into account this leads to $2^4 = 16$ two-body matrix elements. Considering in addition only on-shell matrix elements the number of independent matrix elements can be further reduced by symmetry arguments down to 5. Thus, all on-shell two-body matrix elements can be expanded into five Lorentz invariants. These five invariants are not unique because the Dirac matrices always involve also negative-energy states. Therefore a decomposition of the one-body *NN* potential into a Lorentz scalar and a Lorentz vector contribution depends to some part on the choice of these five Lorentz invariants.

A natural choice of a set of five linearly independent covariant operators to represent a 4×4 Dirac matrix are the scalar, vector, tensor, axial-vector, and pseudoscalar Fermi covariants

$$S = 1 \otimes 1, \qquad V = \gamma^\mu \otimes \gamma_\mu, \qquad T = \sigma^{\mu\nu} \otimes \sigma_{\mu\nu},$$
$$P = \gamma_5 \otimes \gamma_5, \qquad A = \gamma_5\gamma^\mu \otimes \gamma_5\gamma_\mu. \qquad (17)$$

Because one works with physical, i.e., antisymmetrized matrix elements, one has to realize that the Fierz transformation $\mathcal{F}$ [26] couples direct and exchange covariants that mixes the different Lorentz structures

$$\begin{pmatrix} \tilde{S} \\ \tilde{V} \\ \tilde{T} \\ \tilde{A} \\ \tilde{P} \end{pmatrix} = \frac{1}{4} \begin{pmatrix} 1 & 1 & \frac{1}{2} & -1 & 1 \\ 4 & -2 & 0 & -2 & -4 \\ 12 & 0 & -2 & 0 & 12 \\ -4 & -2 & 0 & -2 & 4 \\ 1 & -1 & \frac{1}{2} & 1 & 1 \end{pmatrix} \begin{pmatrix} S \\ V \\ T \\ A \\ P \end{pmatrix}. \quad (18)$$

The covariants on the left-hand side of Eq. (18) are the interchanged Fermi covariants defined in Ref. [26] as

$$\tilde{S} = \tilde{S}S, \quad \tilde{V} = \tilde{S}V, \quad \tilde{T} = \tilde{S}T, \quad \tilde{A} = \tilde{S}A, \quad \tilde{P} = \tilde{S}P, \quad (19)$$

where the operator $\tilde{S}$ exchanges the Dirac indices of particles 1 and 2, i.e., $\tilde{S}u(1)_\sigma u(2)_\tau = u(1)_\tau u(2)_\sigma$. Therefore the direct covariants Γ_m with $m = \{S, V, T, P, A\}$ can be expressed in terms of the exchange covariants $\tilde{\Gamma}_m$ with $m = \{\tilde{S}, \tilde{V}, \tilde{T}, \tilde{P}, \tilde{A}\}$.

In contrast to the *NN* potentials where the pion-nucleon coupling is given by a pseudovector vertex, the set (17), (19) contains the pseudoscalar covariant P. This suggests to replace P in Eqs. (17) and (19) by the corresponding pseudovector covariant

$$PV = \frac{\slashed{q}' - \slashed{q}}{2M}\gamma_5 \otimes \frac{\slashed{q}' - \slashed{q}}{2M}\gamma_5. \qquad (20)$$

This leads to an on-shell equivalence because the matrix elements of the pseudovector and the pseudoscalar matrix

operators are identical in the case of on-shell scattering between positive-energy states:

$$\bar{u}(\mathbf{q}')\frac{\slashed{q}' - \slashed{q}}{2M}\gamma_5 u(\mathbf{q}) = \bar{u}(\mathbf{q}')\gamma_5 u(\mathbf{q}). \qquad (21)$$

However, the PV vertex suppresses a coupling to antiparticles because the overlap matrix elements vanish for on-shell scattering

$$\bar{v}(\mathbf{q}')\frac{\slashed{q}' - \slashed{q}}{2M}\gamma_5 u(\mathbf{q}) = 0. \qquad (22)$$

To identify the PV contributions clearly in the antisymmetrized amplitudes—note that due to the Fierz transformation (18) all operators are coupled—one can switch to a set of covariants originally proposed by Tjon and Wallace [34]. Based on the following operator identities

$$\tfrac{1}{2}(T + \tilde{T}) = S + \tilde{S} + P + \tilde{P} \qquad (23)$$

$$V + \tilde{V} = S + \tilde{S} - P - \tilde{P} \qquad (24)$$

one finds that the following set of covariants

$$\Gamma_m = \{S, \tilde{S}, (A - \tilde{A}), PV, \widetilde{PV}\} \qquad (25)$$

provides a set of Dirac operators for the positive energy sector [34] that completely separates the direct and exchange *pv* contributions from the remaining operator structure. This has the advantage that the OPE exchange that is dominant at low energies is decoupled from the remaining amplitudes and gives only a contribution to the $\widetilde{PV}$ operator. In the following we refer to the set of covariants in Eq. (25) as the *pseudovector* representation and that of Eq. (17) as the *pseudoscalar* representation. Note that on-shell matrix elements of PV, $\widetilde{PV}$ in Eq. (25) are equivalent to those where the pseudovector covariants are replaced by P, $\tilde{P}$.

The on-shell equivalence does not affect physical observables that are built on complete matrix elements as, e.g., the single-particle potential *U*

$$U(\mathbf{k})_{\text{s.p.}} \propto \sum_{\mathbf{q}} \langle \bar{u}(\mathbf{k})\bar{u}(\mathbf{q})|\hat{V}(\mathbf{k}, \mathbf{q})|u(\mathbf{k})u(\mathbf{q}) - u(\mathbf{q})u(\mathbf{k})\rangle, \quad (26)$$

but it leads to uncertainties in operators which are, like the self-energy Σ, based on traces over only one particle. As discussed in Ref. [35], a pseudovector πN coupling leads to the *pseudovector* representation (25) as the most natural choice of the relativistic operator basis.

B. Projection onto the covariant operators

In this section the technique is described necessary to project the Born amplitudes from an angular-momentum basis onto the covariant basis, given by Eqs. (17) or (25). The procedure is standard and runs over the following steps

$$|LSJ\rangle \rightarrow \text{partial wave helicity states}$$
$$\rightarrow \text{plane wave helicity states} \rightarrow \text{covariant basis.}$$

The first two transformation can be found in Refs. [36,37]. The last step depends on the choice of the covariant operator basis; see, e.g. [14,27]. Here we sketch the essential steps briefly.

Independent of the various models, the amplitudes are determined normally in the $|LSJM\rangle$ representation and can be denoted as $V_{L',L}^{JS}(\mathbf{q}', \mathbf{q})$. In case of on-shell scattering ($|\mathbf{q}| = |\mathbf{q}'|$), due to time-reversal invariance and spin and parity conservation, only 5 of 16 possible matrix elements are linearly independent for a fixed total angular momentum J (spin singlet and triplet states). By inversion of Eq. (3.32) in Ref. [36] these five partial-wave amplitudes are transformed from the $|LSJM\rangle$ representation into the partial-wave helicity representation $|JM\lambda_1\lambda_2\rangle$ and are then decoupled via inversion of Eq. (3.28) from Ref. [36]. Because we deal with two-nucleon states that are two-fermion states, we have to evaluate the fully antisymmetrized matrix elements by restoring the total isospin $I = 0, 1$ via the standard selection rule

$$(-1)^{L+S+I} = -1. \tag{27}$$

The five plane-wave helicity matrix elements are then obtained by a summation over the total angular momentum J

$$\langle \lambda_1' \lambda_2' \, \mathbf{q}' | V^I | \lambda_1 \lambda_2 \, \mathbf{q} \rangle = \sum_J \left(\frac{2J+1}{4\pi} \right) d_{\lambda\lambda'}^J(\theta)$$
$$\times \langle \lambda_1' \lambda_2' | V^{J,I}(\mathbf{q}', \mathbf{q}) | \lambda_1 \lambda_2 \rangle. \tag{28}$$

Here θ denotes the scattering angle between $\mathbf{q}'$ and $\mathbf{q}$, whereas $\lambda = \lambda_1 - \lambda_2$ and $\lambda' = \lambda_1' - \lambda_2'$ denote the in- and outgoing helicity states. The reduced rotation matrices $d_{\lambda\lambda'}^J(\theta)$ are those defined by Rose [38].

These plane-wave helicity matrix elements can now be projected onto a set of five covariant amplitudes in Dirac space. A set of five linearly independent covariants is sufficient for such a representation because on-shell we deal with five matrix elements independent of the chosen representation. Using the covariants of Eq. (17) (the "pseudoscalar choice") the on-shell potential matrix elements for definite isospin I can be represented covariantly as [27]

$$\hat{V}^I(|\mathbf{q}|, \theta) = F_S^I(|\mathbf{q}|, \theta) \, S + F_V^I(|\mathbf{q}|, \theta) \, V + F_T^I(|\mathbf{q}|, \theta) \, T$$
$$+ F_P^I(|\mathbf{q}|, \theta) \, P + F_A^I(|\mathbf{q}|, \theta) \, A. \tag{29}$$

The Lorentz invariant amplitudes $F_m^I(|\mathbf{q}|, \theta)$ with $m = \{S, V, T, P, A\}$ from Eq. (29) depend only on the relative c.m. momentum $|\mathbf{q}|$ and the scattering angle θ and are related to the plane-wave helicity states defined in Eq. (28) by

$$\langle \lambda_1' \lambda_2' \, \mathbf{q}' | V^I | \lambda_1 \lambda_2 \, \mathbf{q} \rangle = \sum_m \langle \lambda_1' \lambda_2' \, \mathbf{q}' | \Gamma_m | \lambda_1 \lambda_2 \, \mathbf{q} \rangle F_m^I(|\mathbf{q}|, \theta). \tag{30}$$

The indices (1) and (2) refer to particles 1 and 2. Equation (30) is a matrix relation between the five independent plane-wave helicity amplitudes V_i^I (where $i = \{\lambda_1', \lambda_2', \lambda_1, \lambda_2\} = 1, \ldots, 5$ denotes 5 of 16 possible amplitudes) and the five unknown covariant amplitudes $F_m^I(|\mathbf{q}|, \theta)$. For fixed values of the variables ($|\mathbf{q}| = |\mathbf{q}'|, \theta$) this equation can be written in a more compact form

$$V_i^I = \frac{1}{M^2} \sum_m C_{im} F_m^I. \tag{31}$$

The covariant amplitudes F_m^I are obtained by matrix inversion of Eq. (31) that corresponds to Eq. (3.23) of Ref. [27].

Equation (31) has to be inverted for two scattering angles, i.e., for $\theta = 0$ for the direct and $\theta = \pi$ for the exchange part of the interaction. These two scattering angles are required for the Hartree-Fock potential. Details of the inversion of Eq. (31), as well as the treatment of kinematical singularities of the matrix C_{im} occurring at $\theta = 0$ and $\theta = \pi$ are given in Appendix C of Ref. [27], where Eq. (31) is explicitly given for $\theta = 0$ and $\theta = \pi$ [Eqs. (C10) and (C11)]. Following Ref. [27] we calculate the real part of the five Lorentz invariant amplitudes $F_m^{I=0,1}(|\mathbf{q}|, \theta = 0, \pi)$ for the direct and exchange case in both the isospin singlet and triplet channels. When derived from physical partial-wave amplitudes that are already antisymmetrized according to the selection rule (27), the exchange amplitudes $F_m(|\mathbf{q}|, \pi)$ contain redundant information.

Because we are restricted to the subspace of positive energy states, the choice of a set of five linearly independent covariants suffers from on-shell ambiguities, as discussed above. Thus the set of covariants (25) is a more appropriate choice [14]. In this representation the scattering matrix reads [14,34]

$$\hat{V}^I(|\mathbf{q}|, \theta) = g_S^I(|\mathbf{q}|, \theta) \, S - g_{\tilde{S}}^I|\mathbf{q}|, \theta) \, \tilde{S} + g_A^I(|\mathbf{q}|, \theta) \, (A - \tilde{A})$$
$$+ g_{PV}^I(|\mathbf{q}|, \theta) \, PV - g_{\widetilde{PV}}^I(|\mathbf{q}|, \theta) \, \widetilde{PV}. \tag{32}$$

The new amplitudes g_m^I are related to the Lorentz invariant amplitudes F_m^I from Eq. (29) by the linear transformation

$$\begin{pmatrix} g_S^I \\ g_{\tilde{S}}^I \\ g_A^I \\ g_{PV}^I \\ g_{\widetilde{PV}}^I \end{pmatrix} = \frac{1}{4} \begin{pmatrix} 4 & -2 & -8 & 0 & -2 \\ 0 & -6 & -16 & 0 & 2 \\ 0 & -2 & 0 & 0 & -2 \\ 0 & 2 & -8 & 4 & 2 \\ 0 & 6 & -16 & 0 & -2 \end{pmatrix} \begin{pmatrix} F_S^I \\ F_V^I \\ F_T^I \\ F_P^I \\ F_A^I \end{pmatrix}. \tag{33}$$

As mentioned before, the representation of the potential given in Eq. (32) has the advantage that the OPE contribution to the amplitudes is completely decoupled from the rest of the interaction. The OPE contributes only in the pseudovector exchange amplitude g_{PV}^{OPE} and vanishes in all other amplitudes $g_S^{OPE} = g_{\tilde{S}}^{OPE} = g_A^{OPE} = g_{PV}^{OPE} = 0$. Thus one avoids that the low-momentum behavior of these four amplitudes is to large extent dominated by OPE exchange contributions that are present in all five amplitudes F_m^I from Eq. (29) due to the Fierz transformation. To compare the various potentials at the level of covariant amplitudes the pseudovector representation is therefore the most efficient and transparent one.

C. Covariant amplitudes

To demonstrate the dependence of the relativistic amplitudes on the choice of the operator basis we consider in Fig. 2 first the single OPE. The figure shows the corresponding amplitudes F_m of the pseudoscalar representation (17) and the g_m amplitudes of pseudovector representation (25), both for the OPE part of the Bonn A potential. Because we are dealing with antisymmetrized amplitudes it is sufficient to consider the direct Lorentz invariants $F_m(|\mathbf{q}|, \theta = 0)$ and $g_m(|\mathbf{q}|, \theta = 0)$ at scattering angle $\theta = 0$. As the starting point the OPE is given in the $|LSJ\rangle$ basis and antisymmetrization is ensured by the
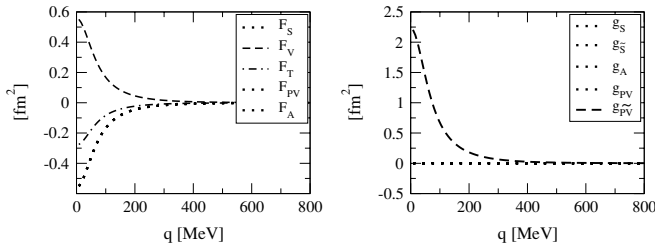
FIG. 2. Covariant amplitudes for the single OPE for the different choices of the relativistic operator basis, i.e., the pseudoscalar representation $F_m(|\mathbf{q}|, \theta = 0)$ (left) and the pseudovector representation $g_m(|\mathbf{q}|, \theta = 0)$ (right).

selection rule (27). The figure shows the isospin averaged amplitudes defined as

$$F_m(|\mathbf{q}|, 0) := \frac{1}{2} \left[F_m^{I=0}(|\mathbf{q}|, 0) + 3 F_m^{I=1}(|\mathbf{q}|, 0) \right] \qquad (34)$$

and correspondingly for g_m. It is evident that in the pseudoscalar representation all amplitudes F_m have large nonvanishing contributions from OPE due to the mixing of direct and exchange contributions described by the Fierz transformation (18). Moreover, as discussed above the on-shell equivalence for the pseudoscalar covariant P and the pseudovector covariant $\widetilde{PV}$ in Eq. (29) leads to identical Lorentz invariant amplitudes $F_{PS} = F_{PV} \equiv F_P$ [14]. The pseudovector representation (25), however, has the advantage that it decouples the OPE contribution from the remaining amplitudes, i.e., the OPE gives a nonzero contribution only in the $g_{\widetilde{PV}}$ amplitude, whereas the others are zero. For the single pion exchange $g_{\widetilde{PV}}$ is now easy to interpret: it is just the pion propagator (3) times the pion-nucleon form factor (2).

When the various NN potentials are compared, this is done most efficiently in the pseudovector representation. All potentials contain an OPE of similar strength that dominates at small momenta. The pseudovector representation decouples the OPE contribution from the remaining amplitudes $g_m \neq g_{\widetilde{PV}}$ and allows thus a more transparent investigation of the short and intermediate range parts of the potentials that are actually the interesting ones. Figure 3 shows the isospin-averaged amplitudes $g_m^D(|\mathbf{p}|, \theta = 0)$ for Bonn A, CD-Bonn, Argonne v_{18}, Nijm93, Nijmegen I and II, Reid93, the effective low-momentum interaction $V_{\mathrm{low}\,k}$ and the chiral Idaho potential. The amplitudes are obtained going through the transformation scheme discussed above. Partial waves are taken into account up to $J = 90$ (Bonn A, CD-Bonn, Idaho), $J = 9$ (Argonne v_{18}, Nijmegen I/II, Nijm93, Reid93) and $J = 6$ ($V_{\mathrm{low}\,k}$).

The amplitudes determined from the complete NN potentials are no more easy to interpret as for a single meson exchange, where they represent essentially the propagators times the form factors. This is also true for the full OBE because the contributions from the various mesons are coupled through their exchange parts. Because these amplitudes are not very transparent quantities, Fig. 3 includes as a reference in addition the contributions from only OPE and from only σ and ω exchange, both taken from Bonn A.

Several features can now be seen from Fig. 3: First, the four amplitudes g_S, $g_{\tilde{S}}$, g_A and $g_{\widetilde{PV}}$ are very close for the OBEPs Bonn A, CD-Bonn, and Nijm93 and the phenomenological nonrelativistic Argonne v_{18} and Nijmegen I/II potentials. Only at very small $|\mathbf{q}|$ Argonne v_{18} shows a deviating structure. The direct pseudovector amplitude g_{PV} falls somewhat out of systematics. This amplitude is, however, of minor importance because it does not contribute to the Hartree-Fock self-energy (41)–(43) and to the single-particle potential.

The dominance of the OPE at low $|\mathbf{q}|$ is reflected in the pseudovector exchange amplitude $g_{\widetilde{PV}}$, which is at small $|\mathbf{q}|$ almost two orders of magnitude larger than the other amplitudes. In the OBEPs the high-momentum part of the interaction, however, is dominated by heavy meson exchange and the corresponding amplitudes g_S, $g_{\tilde{S}}$, g_A approach the $\sigma + \omega$ exchange result. Deviations from the $\sigma + \omega$ amplitudes, e.g., due to exchange of isovector mesons ρ and δ in the OBEPs are moderate at large $|\mathbf{q}|$. These deviations are more pronounced at small $|\mathbf{q}|$.

The remarkable agreement between the OBE amplitudes and those derived from the nonrelativistic Argonne v_{18} potential demonstrates two things: first, it means that for on-shell scattering the Argonne v_{18} can be mapped on the relativistic operator structure where the local phenomenological functions V_i, Eq. (7), play the same role as the meson propagators plus corresponding form factors in the meson exchange picture. Second, the effective treatment of the short-distance physics in Argonne v_{18} is very similar to that in the OBE potentials Bonn A, CD-Bonn, and Nijm93. This fact can be estimated from Fig. 1, where the $^1S_0$ partial-wave amplitudes are close as well. However, the softer character of the Reid93 and also the Nijmegen I and II potentials is reflected clearly in the stronger deviation from the $\sigma + \omega$ amplitudes at large $|\mathbf{q}|$.

Finally we are turning to the effective low-momentum potentials $V_{\mathrm{low}\,k}$ and the chiral Idaho N^{3}LO potential. $V_{\mathrm{low}\,k}$ is only shown up to the intrinsic cutoff of 400 MeV. In this momentum range the amplitudes fall practically on top of those from the Idaho N^{3}LO potential. At low $|\mathbf{q}|$ the amplitudes derived from Idaho N^{3}LO and $V_{\mathrm{low}\,k}$ behave qualitatively and quantitatively like the previous ones, i.e., they are very close to Bonn A, CD-Bonn, and Argonne v_{18}. We conclude that also the effective low-momentum potentials can be mapped on a relativistic operator structure. For the Idaho N^{3}LO potential, which is also based on the operator structure given in Eq. (8), the functions V_i and V_i' in combination with the corresponding operators, derived from fourth-order 2π exchange plus contact terms, lead to a structure that is similar to that imposed by the OBE picture. However, clear deviations appear in the cutoff region between 400 and 500 MeV. The short-range interactions are strongly suppressed by the exponential cutoff form factors and as a consequence the Idaho rapidly approaches the OPE result for momenta above 400 MeV.

IV. SELF-ENERGY IN NUCLEAR MATTER

With the covariant amplitudes at hand, one is able to determine the relativistic mean field in nuclear matter with its scalar and vector components. To do so, we calculate the relativistic self-energy Σ in Hartree-Fock approximation
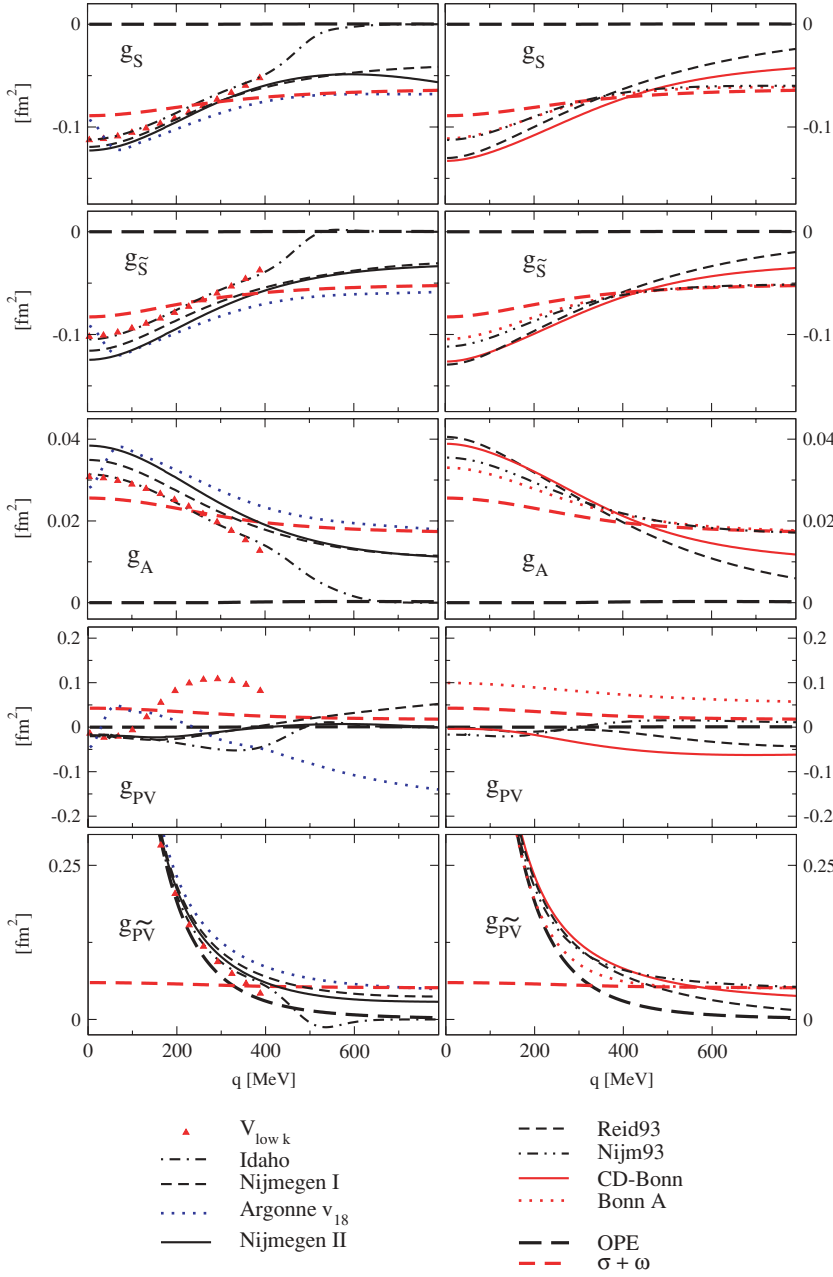
FIG. 3. (Color online) Isospin-averaged Lorentz invariant amplitudes $g_m^D(|\mathbf{q}|, \theta = 0)$ for the different *NN* potentials after projection on the Dirac operator structure. The pseudovector representation of the relativistic operator basis is used. As a reference the amplitudes from solely OPE and from $\sigma + \omega$ exchange, both with Bonn A parameters, are shown.

at *tree level*. We are thereby not aiming for a realistic description of nuclear matter saturation properties that would require a self-consistent scheme. Moreover, short-range correlations require to base such calculations on the in-medium T matrix rather than the bare potential V. This leads to the relativistic Dirac-Brueckner-Hartree-Fock scheme, which has been proven to describe nuclear saturation with quantitatively satisfying accuracy [13–15,47]. The self-consistent iteration of the self-energy in combination with the Dyson equation for the in-medium nucleon propagator and the Bethe-Salpeter equation for the in-medium T matrix leads to self-energy components that are qualitatively of similar magnitude than the tree level results, as will be seen later on.

The self-energy is determined by the summation of the interaction of a nucleon with four-momentum k with all

nucleons inside the Fermi sea in Hartree-Fock approximation

$$\Sigma_{\alpha\beta}(k, k_F) = -i \int \frac{d^4q}{(2\pi)^4} G_{\tau\sigma}^D(q)$$
$$\times [V(|\mathbf{p}|, 0)_{\alpha\sigma;\beta\tau} - V(|\mathbf{p}|, \pi)_{\alpha\sigma;\tau\beta}]. \quad (35)$$

Because we work with fully antisymmetrized matrix elements that contain already the direct (Hartree) and exchange (Fock) contributions, it is sufficient to evaluate the Hartree integral for the self-energy

$$\Sigma_{\alpha\beta}(k, k_F) = -i \int \frac{d^4q}{(2\pi)^4} G_{\tau\sigma}^D(q) [V^A(|\mathbf{p}|, 0)_{\alpha\sigma;\beta\tau}]. \quad (36)$$

$G^D(q)$ is the Dirac propagator describing the on-shell propagation of a nucleon with momentum q inside the Fermi sea in

the nuclear matter rest frame

$$G^D(q) = [\not{q} + M]2\pi i\delta(q^2 - M^2)\Theta(q_0)\Theta(k_F - |\mathbf{q}|). \quad (37)$$

The Θ functions account for the fact that only positive energies are considered. Here, $\mathbf{k}$, taken along the z axis, is the single-particle momentum of the incoming nucleon in the nuclear matter rest frame. The relative momentum in the two-nucleon c.m. frame where the matrix elements V are evaluated is given by $|\mathbf{p}| = \sqrt{s/4 - M^2}$, where $s = [E(\mathbf{k}) + E(\mathbf{q})]^2 - (\mathbf{k} + \mathbf{q})^2$ is the total energy of the two nucleons.

Using the pseudovector representation for the on-shell matrix elements V, Eq. (32), the self-energy operator reads

$$\Sigma_{\alpha\beta}(k, k_F) = \int \frac{d^3\mathbf{q}}{(2\pi)^3} \frac{\Theta(k_F - |\mathbf{q}|)}{4E(\mathbf{q})}$$

$$\times \left\{ (\not{k}_{\alpha\beta} - \not{q}_{\alpha\beta}) \frac{2q_\mu(k^\mu - q^\mu)}{4M^2} g_{\widetilde{PV}} \right.$$

$$+ m 1_{\alpha\beta} \left[4g_S - g_{\tilde{S}} + 4g_A - \frac{(k^\mu - q^\mu)^2}{4M^2} g_{\widetilde{PV}} \right]$$

$$\left. + \not{q}_{\alpha\beta} \left[-g_{\tilde{S}} + 2g_A - \frac{(k^\mu - q^\mu)^2}{4M^2} g_{\widetilde{PV}} \right] \right\}. \quad (38)$$

Translational and rotational invariance, hermiticity, parity conservation, and time-reversal invariance determine the Dirac structure of the self-energy [27]. In the nuclear matter rest frame the self-energy can be written as

$$\Sigma(k, k_F) = \Sigma_s(k, k_F) - \gamma_0\Sigma_0(k, k_F) + \boldsymbol{\gamma} \cdot \mathbf{k}\, \Sigma_v(k, k_F). \quad (39)$$

Note that the sign convention for the vector field $\Sigma = \Sigma_s - \gamma_\mu\Sigma^\mu$ with $\Sigma_\mu = (\Sigma_0, \mathbf{k}\Sigma_v)$ in Eq. (39) is that used standardly in DBHF [12,14,16]. It differs from that used standardly in QHD ($\Sigma = \Sigma_s + \gamma_\mu\Sigma^\mu$) and also that of Eqs. (49) and (51). The self-energy components are Lorentz scalar functions depending on the Lorentz invariants k^2, $k \cdot j$, and j^2, where j_μ denotes the four-vector baryon current. In nuclear matter at rest the timelike component is just the baryon density and spatial components of the current vanish, i.e., $j_\mu = (\rho_B, \mathbf{0})$. Hence, the Lorentz invariants can be expressed in terms of k_0, $|\mathbf{k}|$, and k_F, where k_F denotes the Fermi momentum. The components of the self-energy are computed by taking the respective traces in the Dirac space [27,39]

$$\Sigma_s = \tfrac{1}{4}tr\,[\Sigma], \quad \Sigma_0 = \tfrac{-1}{4}tr\,[\gamma_0\Sigma],$$

$$\Sigma_v = \frac{-1}{4|\mathbf{k}|^2}\, tr\,[\boldsymbol{\gamma} \cdot \mathbf{k}\Sigma]. \quad (40)$$

In doing so, the Lorentz components of the self-energy operator (38) are given by

$$\Sigma_s(k, k_F) = \frac{1}{4} \int \frac{d^3\mathbf{q}}{(2\pi)^3} \Theta(k_F - |\mathbf{q}|) \frac{M}{E(\mathbf{q})}$$

$$\times \left[4g_S - g_{\tilde{S}} + 4g_A - \frac{(k^\mu - q^\mu)^2}{4M^2} g_{\widetilde{PV}} \right], \quad (41)$$
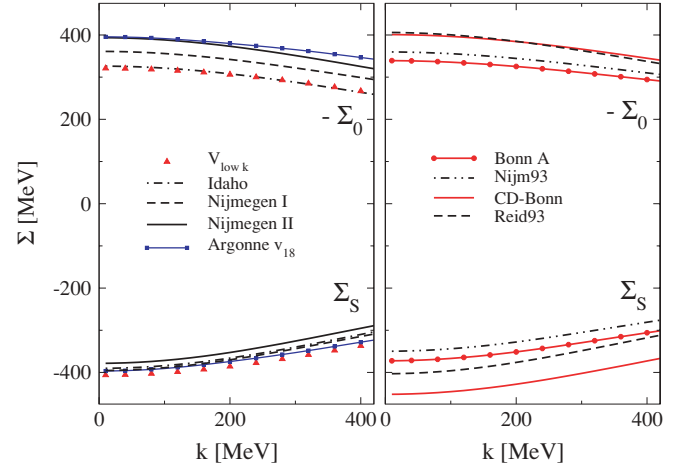

FIG. 4. (Color online) Tree-level scalar and vector self-energy components in nuclear matter at $k_F = 1.35\,\text{fm}^{-1}$ obtained with different *NN* interaction models.

$$\Sigma_0(k, k_F) = \frac{1}{4} \int \frac{d^3\mathbf{q}}{(2\pi)^3} \Theta(k_F - |\mathbf{q}|)$$

$$\times \left[g_{\tilde{S}} - 2g_A + \frac{E(\mathbf{k})}{E(\mathbf{q})} \frac{(k^\mu - q^\mu)^2}{4M^2} g_{\widetilde{PV}} \right] \quad (42)$$

and

$$\Sigma_v(k, k_F) = \frac{1}{4} \int \frac{d^3\mathbf{q}}{(2\pi)^3} \Theta(k_F - |\mathbf{q}|) \frac{\mathbf{k} \cdot \mathbf{q}}{|\mathbf{k}|^2 E(\mathbf{q})}$$

$$\times \left[g_{\tilde{S}} - 2g_A + \frac{k_z}{q_z} \frac{(k^\mu - q^\mu)^2}{4M^2} g_{\widetilde{PV}} \right]. \quad (43)$$

In Fig. 4 the tree-level scalar and vector self-energy components in nuclear matter are shown obtained with the various *NN* potentials at nuclear saturation density with Fermi momentum $k_F = 1.35\,\text{fm}^{-1}$, which corresponds to a density of $\rho = 0.166\,\text{fm}^{-3}$. As a remarkable result, all potentials yield scalar and vector mean fields Σ_s and Σ_0 of comparable strength: a large and attractive scalar field $\Sigma_s \simeq -(450 \div 400)$ MeV and a repulsive vector field of $-\Sigma_0 \simeq +(350 \div 400)$ MeV. These values are comparable to those derived from RMF phenomenologically and also from QCD sum rules. Also the explicit momentum dependence of the self-energy is similar for the various potentials. The Idaho mean fields follow the other approaches at low k but show a stronger decrease above $k \simeq 2\,\text{fm}^{-1}$, which reflects again the influence of the cutoff parameter. Figure 5 shows the spatial component of the vector self-energy $\mathbf{k}\Sigma_v$, Eq. (43). Also here the various potentials agree quite well. As known from self-consistent DBHF calculations [12,14], the spatial vector self-energy is a moderate correction to the large scalar and timelike vector components Σ_s and Σ_0. This is found to be also the case at tree level where $\mathbf{k}\Sigma_v$ is about one order of magnitude smaller than the other two components. The spatial self-energy originates exclusively from exchange contributions, i.e., the Fock term, and vanishes, e.g., in the mean-field approximation of RMF theory.
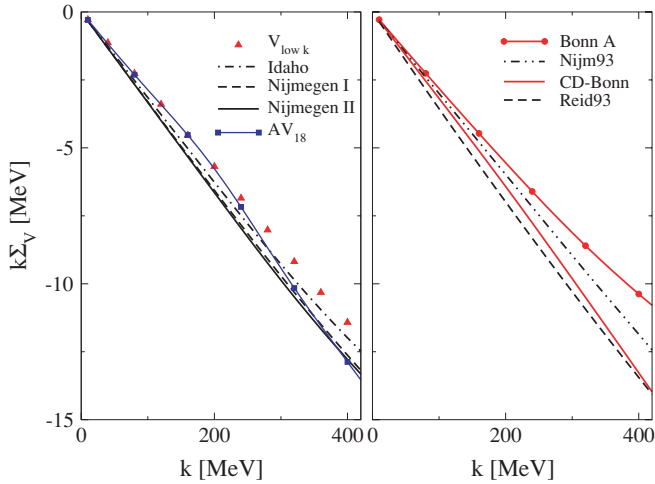
FIG. 5. (Color online) Tree-level spatial vector self-energy component $\mathbf{k}\Sigma_v$ in nuclear matter at $k_F = 1.35\,\mathrm{fm}^{-1}$ for the various potentials.

Figure 6 displays the density dependence of the fields, evaluated at momentum $k = k_F$. At moderate densities the different potentials yield scalar and vector fields that are rather close in magnitude. At higher densities the results start to split up, which reflects again the different treatment of short distance physics in the various interactions. Only the two low-momentum interactions Idaho N^3LO and $V_{low\,k}$ lie practically on top of each other. In this context we want to stress again that these results are obtained in lowest order in density. Hence, the results are "realistic" only in the low-density limit but not at higher densities because short-range correlations are missing.

To estimate the influence of short-range correlations and self-consistency, in Fig. 7 the tree-level result from Fig. 4 for Bonn A to a corresponding full DBHF calculation are compared at $k_F = 1.35\,\mathrm{fm}^{-1}$. For DBHF the approach of Ref. [14] is used (subtracted T matrix in pv representation).
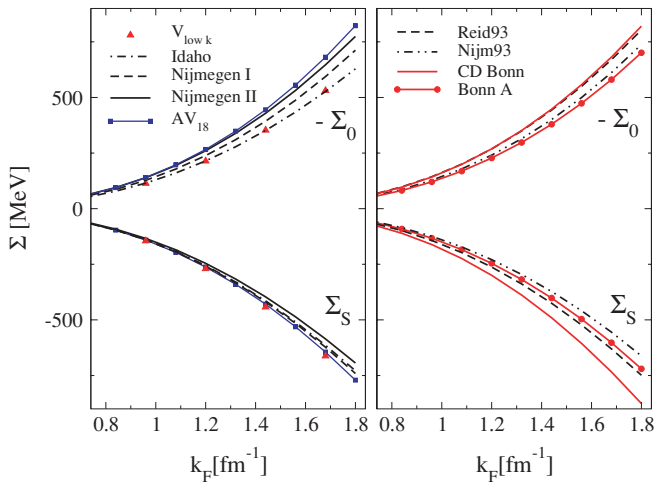

FIG. 6. (Color online) Density dependence of the tree-level scalar and vector self-energy components in nuclear matter obtained with the various potentials.
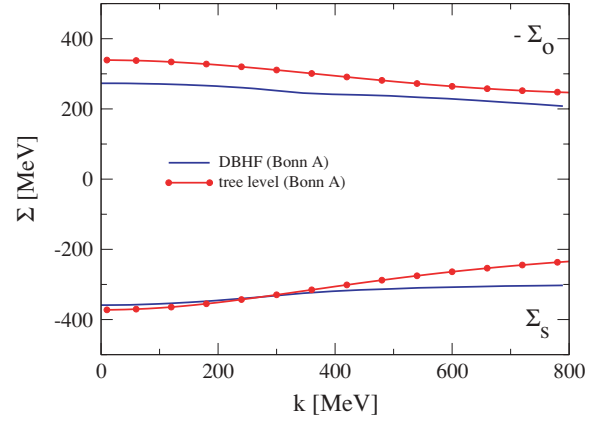

FIG. 7. (Color online) Tree-level scalar and vector self-energy components in nuclear matter at $k_F = 1.35\,\mathrm{fm}^{-1}$ are compared to corresponding values from a full self-consistent relativistic Brueckner (DBHF) calculation. In both cases the Bonn A potential is used.

The DBHF calculation yields reasonable saturation properties with a binding energy of $E_{bind} = -15.72$ MeV and a saturation density of $\rho = 0.181\,\mathrm{fm}^{-3}$ [14]. It is no doubt that higher-order correlations are essential for saturation of nuclear matter. The correlations lead to a general reduction of the vector self-energy by a shift of about 70 MeV. Self-consistency and correlations also weakens the momentum dependence, in particular for Σ_s. However, except of the 70 MeV shift of Σ_0, the absolute magnitude of the self-energies is not strongly modified in the realistic calculation. This means that one can expect that the large attractive scalar and repulsive vector mean fields will also persist for the other interactions when short-range correlations are accounted for in a full relativistic many-body calculation.

Figure 8 shows finally the single-particle potential in nuclear matter at $k_F = 1.35\,\mathrm{fm}^{-1}$, determined from the
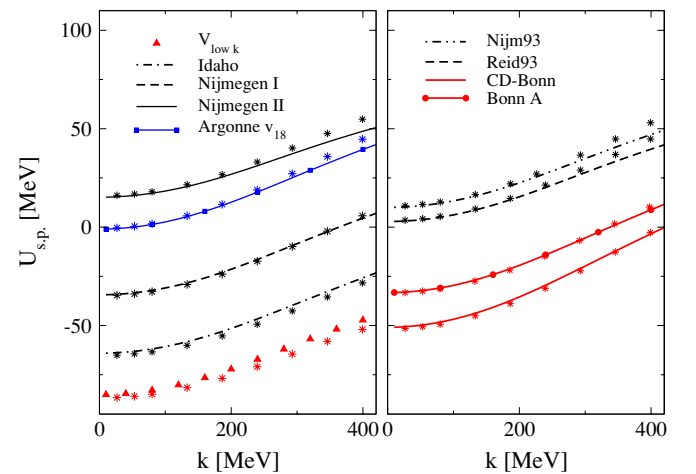

FIG. 8. (Color online) Single-particle potential in nuclear matter at $k_F = 1.35\,\mathrm{fm}^{-1}$, determined from the tree-level Born amplitudes of the various potentials. The single-particle potential determined from the relativistic self-energy components after projection onto the covariant operator basis is compared to a nonrelativistic calculation (stars) where partial-wave amplitudes are summed up directly.

relativistic self-energy components. The single-particle potential is defined as the expectation value of the self-energy

$$U_{\text{s.p.}}(k, k_F) = \frac{\langle u(k)|\gamma^0 \Sigma|u(k)\rangle}{\langle u(k)|u(k)\rangle}$$
$$= \frac{M}{E(\mathbf{k})}\langle \bar{u}(k)|\Sigma|u(k)\rangle \qquad (44)$$

and reads

$$U_{\text{s.p.}}(k, k_F) = \frac{M}{E}\Sigma_s - \frac{k_\mu \Sigma^\mu}{E}$$
$$= \frac{M\Sigma_s}{\sqrt{\mathbf{k}^2 + M^2}} - \Sigma_0 + \frac{\Sigma_v \mathbf{k}^2}{\sqrt{\mathbf{k}^2 + M^2}}. \qquad (45)$$

Equation (45) represents the single particle potential at tree level, i.e., the expectation value of Σ with the bare spinor basis. The next step towards a self-consistent treatment would be to use an in-medium spinor basis which includes the scalar and vector self-energy components via effective masses and effective four-momenta

$$M^*(k, k_F) = M + \Sigma_s(k, k_F), \quad k_\mu^* = k_\mu + \Sigma_\mu(k, k_F). \qquad (46)$$

This would, however, involve higher-order corrections in the baryon density and is not intended in the present investigations that are restricted to leading oder.

The single-particle potential reflects the well-known fact that phase-shift equivalent two-body potentials that describe *NN*-scattering data with about the same accuracy [30] can be rather different [30]. This can already be seen from Fig. 1 where the $^1S_0$ matrix elements of the various potentials are shown. The differences are mainly due to a different treatment of the short-range part of the nuclear interaction, i.e., the hard core that is not well constrained by scattering data. Thus the various potentials lead to about the same T matrices when iterated in the Lippmann-Schwinger or Bethe-Salpeter equation. However, at tree level the hard core contributes fully to $U_{\text{s.p.}}$, which explains the shift of the various results in Fig. 8. Integrating out the high-momentum components, e.g., by renormalization group methods, one arrives at equivalent low-momentum potentials $V_{\text{low } k}$ [25]. Because $V_{\text{low } k}$ contains no significant contributions from the hard core it gives already at tree level a realistic single-particle potential. The situation is similar for the chiral EFT N^{3}LO Idaho potential. As can be seen from Fig. 1 Idaho is rather close to $V_{\text{low } k}$, not only in the $^1S_0$ partial wave, and correspondingly both lead to comparable potentials. However, the slight shift of about 10 MeV between $V_{\text{low } k}$ and Idaho reflects again the subtle cancellation effects between the large scalar/vector fields, because at the scale of the fields, Fig. 6, both lie practically on top of each other.

In the present context the single-particle potential serves as an important check of the whole procedure. In Fig. 8 the single-particle potential $U_{\text{s.p.}}$ is shown, calculated from Eq. (45), i.e., after projecting the *NN* potentials from the partial-wave basis onto the covariant operator basis, determining then the relativistic self-energy components and finally $U_{\text{s.p.}}$. Figure 8 includes also the results from a "nonrelativistic" calculation of $U_{\text{s.p.}}$ where the partial-wave amplitudes are directly summed up. To do so we used a nonrelativistic Brueckner-Hartree-Fock program [40] and determined the

single-particle potential in Born approximation. The nonrelativistic results are represented by stars in Fig. 8 and shown to a momentum of 400 MeV. This avoids distortions from nonrelativistic kinematics that occur at higher momenta. At moderate momenta the nonrelativistic and the relativistic calculations show an excellent agreement that demonstrates the accuracy of the applied projection techniques. One has thereby to keep in mind that $U_{\text{s.p.}}$ originates in the relativistic approach from the cancelation of the two scalar and vector fields that are both of the order of about 400 MeV.

V. THE STRUCTURE OF THE SELF-ENERGY FROM CHIRAL EFT

With the projection formalism at hand one is now able to investigate the connection between the appearance of the matter fields and chiral dynamics in more detail. It allows in particular a straightforward and transparent discussion of the contributions that arise at different orders in the chiral expansion of the *NN* interaction, see Eqs. (14) and (15). Such an investigation allows also the building of the bridge to the reduction of the in-medium quark condensates, which is usually interpreted as a signature for a partial restoration of chiral symmetry.

A. Role of contact terms

We are now in the situation to calculate the relativistic scalar and vector self-energies from a chiral EFT nucleon-nucleon potential order by order. For this purpose we apply again the chiral Idaho potential [44]. This allows a separation of the contributions from different orders in the chiral expansion of the *NN* interaction and provides a connection to the low-energy constants (LECs) that appear at the different orders.

Figure 9 shows the tree-level results for the scalar and vector self-energy components in nuclear matter at $k_F = 1.35\,\text{fm}^{-1}$ obtained in leading order (LO) up to next-to-next-to-next-to-leading order (N^{3}LO).
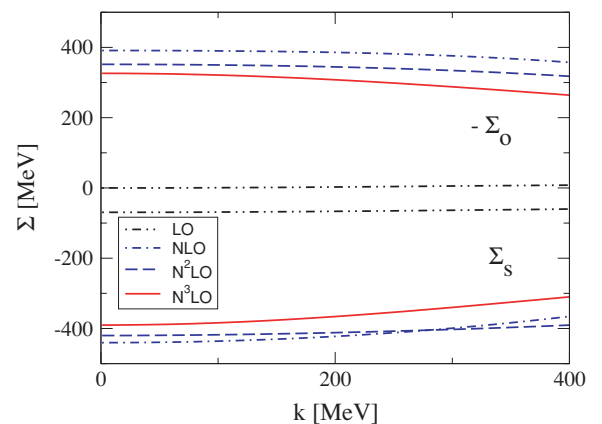

FIG. 9. (Color online) Tree-level scalar and vector self-energy components in nuclear matter at $k_F = 1.35\,\text{fm}^{-1}$ obtained with the chiral EFT *NN* interaction [23]. The fields obtained in leading order (LO) up to next-to-next-to-next-to-leading order (N^{3}LO) are shown.

TABLE I. Contributions from pion dynamics and contact terms to the scalar and vector self-energy components (in MeV) that appear at different orders in the chiral expansion. The evaluation is performed at nuclear saturation density $k_F = 1.35 \, \text{fm}^{-1}$.

	Σ_s	$\Sigma_s^{(\pi)}$	$\Sigma_s^{(\text{cont})}$	$-\Sigma_0$	$-\Sigma_0^{(\pi)}$	$-\Sigma_0^{(\text{cont})}$
LO	-64.76	17.14	-81.9	4.49	19.02	-14.53
NLO	-344.22	4.4	-348.62	376.47	5.16	371.31
N^{2}LO	2.06	2.06	0	-41.92	-41.92	0
N^{3}LO	56.82	-89.34	146.16	-43.27	79.06	-122.33
Sum	-350.1	-65.74	-284.36	295.77	61.32	234.45

To leading order the chiral *NN* interaction does not generate significant mean fields. The scalar self-energy Σ_s is of the order of about -70 MeV and the vector self-energy is practically zero. At LO only the static OPE and contact terms without derivatives appear that involve the operators O_1 and O_2 from the operator basis (8). Hence at LO no pieces from vector exchange occur that would involve all operators $O_i, i = 1 \ldots 5$. The small scalar field means, however, that the nucleon mass M^*, Eq. (46), does not change significantly in matter to leading order in chiral EFT. The dominant contributions arise at next-to-leading order (NLO). NLO involves leading two-pion exchange (2PE) and contact terms with two derivatives. The NLO contact terms contain the full operator structure O_i. At this level both, scalar and vector self-energy components of about ∓ 400 MeV magnitude are generated. Also the signs, i.e., the attractive scalar and the repulsive vector mean field, are fixed at NLO. The higher orders, N^{2}LO and N^{3}LO, provide corrections that tend to reduce the NLO result, are, however, moderate. N^{2}LO contains subleading 2PE and no contact terms at all, whereas N^{3}LO contains subsubleading 2PE, leading three-pion exchange, corrections to OPE and 2PE and contact terms with four derivatives [24].

To investigate the role of pion dynamics and that of contact terms in more detail, Table I contains the contributions that arise from pion dynamics $\Sigma^{(\pi)}$, i.e., OPE, 2PE, 3PE, and corrections, and those from the contact terms $\Sigma^{(\text{cont})}$ separately. The contributions to the self-energy at a particular order is given by the sum $\Sigma^{(\pi)} + \Sigma^{(\text{cont})}$, the full self-energy at a certain order ν is obtained by adding the contributions from the lower orders $\Sigma^{(\nu)} = \sum_{\lambda=0}^{\nu} \Sigma^{(\lambda)}$. From Table I it becomes evident that the dominant contributions to the scalar and vector self-energy are generated by the contact terms that arise at next-to-leading order. At N^{2}LO no contact terms occur in the chiral expansion. The N^{3}LO contacts provide sizable corrections to both scalar and vector self-energy components and are of opposite sign than the NLO contributions. The contribution from pion dynamics to the self-energy components are found to be generally moderate. The largest contributions appear at N^{3}LO and are of opposite sign than those from corresponding contact terms.

Hence the reduction of the nucleon mass $M^* = M + \Sigma_s$ is driven by short-distance physics, dominantly by contact terms that occur at NLO. These are four-nucleon contacts with two derivatives. At this order the short-range spin-orbit interaction

[proportional to O_4 in Eq. (8)]

$$i C_5 (\boldsymbol{\sigma}_1 + \boldsymbol{\sigma}_2) \cdot (\mathbf{q} \times \mathbf{q}') \qquad (47)$$

is generated. The appearance of large scalar/vector fields at NLO is therefore in perfect agreement with Dirac phenomenology where the large spin-orbit force is intimately connected to the appearance of the scalar/vector fields that are generated by short-range isoscalar scalar (σ) and vector meson (ω) exchange [14,47]. In EFT the strength of the short-range spin-orbit interaction is determined by the C_5 parameter that is given by a linear combination of the ^3P-wave low-energy constants (LECs) [23,24]

$$C_5 = \frac{1}{16\pi} [2C_{3P0} + 3C_{3P1} - 5C_{3P2}]. \qquad (48)$$

Hence the short-range spin-orbit interaction is dictated by *P*-wave *NN* scattering. As shown by Kaiser [52] the large values of the C_5 parameter is in good agreement with corresponding values extracted from high-precision OBE-type potentials (Bonn, CD-Bonn, Nijm93, Nijmegen I,II) and from Argonne v_{18}, which are all in the range of $3C_5/8 \sim 80 \div 90$ MeVfm^5. In Ref. [52] these values were also compared to purely phenomenological Skyrme-type density functionals designed for nuclear structure calculations [53,54]. The values of the corresponding spin-orbit strength parameter W_0 in Skyrme models are also very close in magnitude, i.e., $3W_0/4 \sim 75 \div 97$ MeV fm^5. The contribution from chiral OPE to the spin-orbit terms in the density functional were found to be almost negligible (less than 1%). The lowest-order irreducible 2PE that occurs at NLO in the chiral expansion provides moderate corrections to the isoscalar spin-orbit strength function, whereas the isovector strength is more strongly affected (2PE contributions lead to a $\sim$30% reduction) [52]. Thus the analysis of Kaiser is fully consistent with the small fields $\Sigma_s^{(\pi)}$ and $\Sigma_0^{(\pi)}$ of $\sim \mp 5$ MeV generated by pion dynamics at NLO, as observed within the framework of the present analysis.

Figure 10 shows the dependence of the fields on the value of the C_5 low-energy constant in more detail. As already mentioned, at LO two contact terms (C_1 and C_2) appear and at NLO, respectively, five contacts (C_3 to C_7). The figure contains the full NLO result, including contributions from LO and NLO pion dynamics and contacts and compares this to the case where all contacts that appear up to NLO were switched off except of the C_5 contribution. It contains in addition results
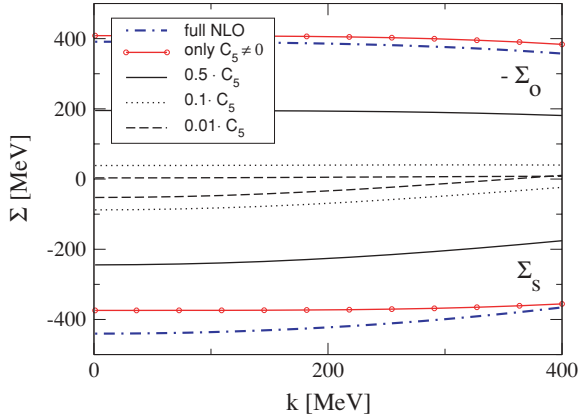
FIG. 10. (Color online) Influence of the C_5 low energy constant. The figure compares the self-energies at NLO to those where all contacts except of C_5 are switched off and those results where the strength of the C_5 parameter is varied.

with again all contributions, scaling the value of C_5 down to 50, 10, and 0.1%. It becomes evident that the large scalar and vector mean fields are a direct consequence of the large value of C_5. Chiral EFT is therefore not only in qualitative but also quantitative agreement with the picture known from meson exchange. In both cases the fields are related to short distance physics and their strength is dictated by P-wave NN-scattering data where the spin-orbit forces occur.

B. Connection to QCD sum rules

In finite-density QCD sum rules scalar and vector fields arise naturally from the structure of the quark propagator that is proportional to the corresponding condensates. As shown by Cohen *et al.* [6] the quark correlation function can be expressed to leading order in terms of the scalar condensate $\langle \rho | \bar{q}q | \rho \rangle$ already present in vacuum, and the vector condensate $\langle \rho | q^\dagger q | \rho \rangle$ that is introduced by the breaking of Lorentz invariance due to the presence of the medium. The identification of the correlation function with the in-medium nucleon propagator of a dressed quasiparticle leads to scalar and vector self-energies Σ_s and Σ_0 that are of the same order in the condensates [6]

$$\Sigma_s = -\frac{8\pi^2}{\Lambda_B^2}[\langle \rho | \bar{q}q | \rho \rangle - \langle \bar{q}q \rangle] = -\frac{8\pi^2}{\Lambda_B^2}\frac{\sigma_N}{m_u + m_d}\rho_S \quad (49)$$

$$-\Sigma_0 = -\frac{64\pi^2}{3\Lambda_B^2}\langle \rho | \bar{q}\gamma_0 q | \rho \rangle = -\frac{32\pi^2}{\Lambda_B^2}\rho. \quad (50)$$

These expression are of leading order in density. ρ_S in Eq. (49) is the scalar nucleon density, $f_\pi = 93$ MeV the weak pion decay constant, and $m_{u,d}$ are the current quark masses of about $5 \div 10$ MeV. The pion-nucleon σ term $\sigma_N = \langle N | m_u \bar{u}u + m_d \bar{d}d | N \rangle$ is determined by the u- and d-quark content of the nucleon and represents the contribution from explicit chiral symmetry breaking to the nucleon mass through the small but nonvanishing current quark masses. It has an empirical value of about $\sigma_N \simeq 50$ MeV. The Borel mass scale $\Lambda_B \simeq 4\pi f_\pi \simeq 1$ GeV is the generic low-energy scale of

QCD that separates the nonperturbative from the perturbative regime. It coincides with the chiral symmetry breaking scale Λ_χ of ChPT. Applying Ioffe's formula [8] for the nucleon mass $M \simeq -8\pi^2/\Lambda_B^2 \langle \bar{q}q \rangle$ one finally obtains the fields in the form [9]

$$\Sigma_s(\rho) = -\frac{\sigma_N M}{m_\pi^2 f_\pi^2}\rho_S, \quad (51)$$

$$-\Sigma_0(\rho) = \frac{4(m_u + m_d)M}{m_\pi^2 f_\pi^2}\rho. \quad (52)$$

However, the dependence of the nucleon mass in matter on the quark condensate is not as straightforward as Eq. (51) suggests. Concerning the in-medium condensate one has carefully to distinguish between contributions from the pion cloud and those of nonpionic origin [41,42].

As pointed out by Birse [41] a naive direct dependence of the nucleon mass on the quark condensate through Eq. (51) leads to contradictions with chiral power counting. The contributions from low-momentum virtual pions that enter the in-medium condensate should not contribute by the same amount to the change of the nucleon properties in matter. They can therefore not as easily be associated with a partial restoration of chiral symmetry as the mean-field approximation, Eqs. (51) and (52), would suggest. This problem has also been investigated by Chanfray *et al.* [42] in the framework of the linear σ model. In their studies the authors were able to reconcile the phenomenology of quantum hadron dynamics with chiral theory, in that case the linear σ model. Their conclusion was that, in contrast to the scalar condensate $\langle \rho | \bar{q}q | \rho \rangle$ that is driven by the σ field, i.e., the chiral partner of the pion, the lowering of the nucleon mass M^* is driven by a chiral invariant scalar field that corresponds to fluctuation along the chiral circle. With other words, the condensate is, to a large extent, reduced by the pion cloud surrounding the nucleons, whereas the nucleon mass is not.

To set up the context for the following discussion, we briefly outline the argumentation of Birse [41]: From Eq. (51) it follows that the effective nucleon mass $M^* = M + \Sigma_s(\rho)$ is directly proportional to the nucleon sigma term

$$M^* = M\left(1 - \frac{\sigma_N}{m_\pi^2 f_\pi^2}\rho_S\right). \quad (53)$$

The chiral expansion of the σ term leads to [43]

$$\sigma_N = Am_\pi^2 - \frac{9}{16\pi}\left(\frac{g_{\pi NN}}{2M}\right)^2 m_\pi^3 + \cdots \quad (54)$$

In the chiral limit the pion-nucleon coupling is connected to the axial vector coupling by the Goldberger-Treiman relation $g_{\pi NN} = g_A M/f_\pi$. The coefficient A involves counter terms related to short-distance physics, whereas the nonanalytic $\mathcal{O}(m_\pi^3)$ term arises purely from long-distance physics of the pion cloud. Inserting Eq. (54) into Eq. (53) implies a dependence of the effective nucleon mass M^* on the pion mass that is of order $\mathcal{O}(m_\pi)$.

At the mean-field level, i.e., in $T - \rho$ approximation, the scalar self-energy (41) is given by the scalar forward-scattering amplitude $T_s(\mathbf{q} = 0)$ [$T_s(\mathbf{q} = 0)$ in Eq. (55) corresponds to the
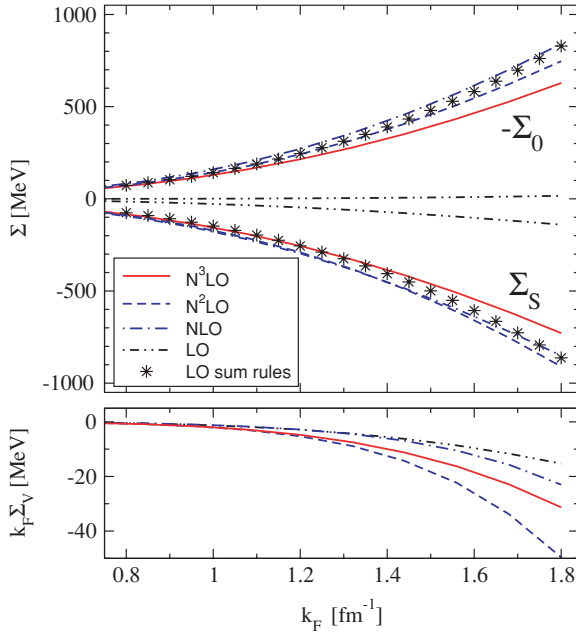
FIG. 11. (Color online) Density dependence of the tree-level scalar and vector self-energy components in nuclear matter obtained with the chiral EFT *NN* interaction [23]. The fields obtained in leading order (LO) up to next-to-next-to-next-to-leading order (N³LO) are shown. The results from leading order QCD sum rules are shown as well.

direct amplitudes F_S and g_S in Eq. (29) and [(32), respectively]

$$\Sigma_s(k_F) = T_s(\mathbf{q} = 0)\rho. \tag{55}$$

A comparison of Eq. (55) with Eqs. (53) and (54) would imply that the scalar part of the forward-scattering amplitude contains a constant and a term of order m_π. Such a dependence contradicts, however, chiral power counting. In chiral EFT the leading term in the pion mass in the *NN* interaction originates from the low-energy expansion of the OPE and is of order $\mathcal{O}(m_\pi^2)$ [22–24]. Hence the *NN* interaction cannot contain a term directly proportional to σ_N/f_π^2.

For the comparison of the sum-rule predictions we turn to the density dependence of the self-energy. Figure 11 shows the density dependence of the fields from the various orders. As in Fig. 6, the scalar Σ_s, timelike vector Σ_0 and spatial vector Σ_v self-energies are determined at momentum $k = k_F$. The density dependence is shown up to $k_F = 1.8\,\text{fm}^{-1}$ that corresponds to about 2.5 times nuclear saturation density. As can be seen from Fig. 11 the relative contributions from the various orders remain the same over the entire density range considered. For comparison the figure contains also the corresponding fields as predicted by leading order QCD sum rules, i.e., Eqs. (51) and (52). For the evaluation of Eq. (51) the empirical value of $\sigma_N = 50$ MeV has been chosen for the nucleon σ term, $f_\pi = 93$ MeV and $(m_u + m_d) = 12$ MeV. For the evaluation of the scalar field in Eq. (51) we have set the scalar density equal to the vector density, i.e., $\rho_s \simeq \rho$.

Both the QCD sum rule and the chiral EFT fields are very comparable in terms of a density expansion because both are obtained to leading order in density. In the case of the sum rules this corresponds to a Fermi gas of noninteracting nucleons. To go beyond the Fermi gas approximation would require including higher-order terms in the operator product expansion and the density expansion of the condensates [6,7,45]. In the EFT case higher orders in density can be introduced by a self-consistent dressing of the interaction (see discussion in Sec. VI) and of course by higher order terms in perturbation series that would finally end up in a full resummation of the Brueckner ladder diagrams.

At moderate nuclear densities the agreement between the QCD sum rules and N³LO is quite remarkable. At higher densities the results from the sum rules tend to overshoot the N³LO values which is, however, not too astonishing because the relations (51) are valid in the low-density limit.

In view of the fact that in chiral *NN* dynamics the fields are dominantly generated by NLO contact terms, one could be tempted to interpret the present results in the way that the reduction of the quark condensates occurs at NLO in the chiral expansion. However, as discussed above such an interpretation is not straightforward. A closer inspection of the terms that drive the sum-rule result reveals the following: the coefficient A in Eq. (54) is related to the unknown coupling C_1 in the effective ChPT pion-nucleon Lagrangian [48]. Becher and Leutwyler extracted a value of $A = 3.7\,\text{GeV}^{-1}$ fitting the elastic πN-scattering amplitude at threshold [49]. Inserting this value into the sum-rule expression (53) corresponds to a scalar self-energy (at $k_F = 1, 35\,\text{fm}^{-1}$) of $\Sigma_s = -513$ MeV at order m_π^0. At order m_π, i.e., when the $\mathcal{O}(m_\pi^3)$ term in the expansion (54) is included, the σ term of 46.7 MeV is already close to its empirical value and a self-energy of $\Sigma_s = -340$ MeV is obtained. Although this value for Σ_s is astonishingly close to the NLO result from chiral *NN* scattering, one has to keep in mind that already the LO result is of order m_π^2 in the pion mass. In contrast to the sum-rule approach there appears no significant repulsive contribution from pion dynamics that would correspond to the $\mathcal{O}(m_\pi^3)$ term in Eq. (54).

The present results are therefore in qualitative agreement with the findings of Refs. [41,42], namely that long-distance physics related to pion dynamics plays only a minor role for the reduction of the nucleon mass in matter. When relating the in-medium nucleon mass to the in-medium scalar condensate through expression (53) one should be very careful. Although the sum-rule mean fields, Eqs. (49) and (50), provide a reasonable approximation to the mean fields from chiral EFT, both approaches do not reflect the same physical concepts. The sum-rule approach assumes that the nucleon properties are determined by the interaction with the in-medium condensates, whereas conventional many-body approaches assume that the in-medium properties are determined by the interaction between the nucleons.

VI. EQUATION OF STATE

Until now all calculations in this article have been performed at *tree level*. It is, however, a well-known fact that a realistic description of nuclear dynamics requires correlations

beyond Hartree-Fock. Short-range correlations are known to be essential for nuclear binding whenever realistic interactions are used. This leads in lowest order of the Brueckner hole-line expansion to the ladder approximation of the Bethe-Goldstone equation for the in-medium G matrix [10], or the Bethe-Salpeter equation in the relativistic case [11]. In contrast to nonrelativistic BHF where the saturation points of isospin saturated matter are allocated on the so-called *Coester* line, the relativistic Dirac-Brueckner-Hartree-Fock approach leads to rather reasonable saturation properties [12–14]. For a review see Ref. [55].

In Hartree-Fock the matter turns out to be unbound, in particular when high-precision potentials with a relatively strong repulsive hard core are applied, e.g., OBE-type potentials or Argonne v_{18}. The situation is qualitatively different for low-momentum interactions ($V_{\text{low }k}$, Idaho N^{3}LO) where the hard core is strongly suppressed by the high-momentum cutoffs. For these interactions isospin saturated nuclear matter collapses and Brueckner ladder correlations do not improve on this situation [50]. Here the matter has to be stabilized by the inclusion of repulsive three-body forces [51]. Doing so, there appears a strong cutoff dependence at tree level that can be removed when the second-order term of the Brueckner perturbation series is added. $V_{\text{low }k}$ in combination with three-body forces does not require a full resummation of the ladder diagrams but can already be treated within second-order perturbation theory [51].

In the present work we do not aim for a fully realistic description of the nuclear many-body problem but restrict the investigations to the Hartree-Fock level. The tree-level results discussed until now are of leading order in density ρ. Higher-order corrections in density can be taken into account when the bare potential matrix elements are replaced by in-medium matrix elements $V \mapsto V^*$. In the relativistic approach such a treatment is well defined. It means evaluating the corresponding Feynman amplitudes (5) through an in-medium spinor basis $u_\lambda^*(k)$ where the nucleons are dressed by the self-energy. Such a treatment requires, however, a definite structure of the interaction that allows evaluating corresponding in-medium amplitudes. It is therefore at present restricted to OBE-type potentials.

The dressing of the interaction through the self-energy leads automatically to a self-consistency problem that is, e.g., solved within DBHF. The higher-order density dependences which are introduced by such a procedure are considered to be one of the essential reasons for the improved saturation behavior of relativistic DBHF compared to nonrelativistic BHF. In the following we study the role of self-consistency at the Hartree-Fock level.

As already mentioned, in a relativistic framework one uses an in-medium spinor basis where the scalar and vector self-energy components from Sec. IV enter via effective masses and momenta, see Eq. (46). Furthermore the spatial vector self-energy component is usually absorbed introducing reduced effective masses and momenta

$$\tilde{M}^* = \frac{M^*}{1 + \Sigma_v}, \quad \tilde{k}_\mu^* = \frac{k_\mu^*}{1 + \Sigma_v}. \tag{56}$$

Hence the kinetic energy can be written as

$$\tilde{k}_0^* = \tilde{E}^* = \frac{E^*}{1 + \Sigma_v} = \sqrt{\mathbf{k}^2 + \tilde{M}^{*2}} \tag{57}$$

and the in-medium spinors of helicity λ are given by

$$u_\lambda^*(k) = \sqrt{\frac{\tilde{E}^* + \tilde{M}^*}{2\tilde{M}^*}} \begin{pmatrix} 1 \\ \frac{2\lambda|\mathbf{k}|}{\tilde{E}^* + \tilde{M}^*} \end{pmatrix} \chi_\lambda. \tag{58}$$

Thus the effective mass $\tilde{M}^*$ introduces a density dependence into the interaction. The effective mass is, however, in general not only density but also momentum dependent. Based on the observation that this explicit momentum dependence is moderate, it is usually neglected and $\tilde{M}^*$ is fixed at the reference point $|\mathbf{k}| = k_F$. In the so-called *reference spectrum approximation* the reduced effective mass $\tilde{M}_F^* = \tilde{M}^*(|\mathbf{k}| = k_F, k_F)$ serves as an iteration parameter. $\tilde{M}^*$ is then the solution of the nonlinear equation

$$\tilde{M}^* = M + \Sigma_s(k_F, \tilde{M}^*) - \tilde{M}^* \Sigma_v(k_F, \tilde{M}^*), \tag{59}$$

which follows from the formulas above. Self-consistency is now achieved by determining for a given start value of $\tilde{M}^*$ the in-medium matrix elements $V_{L',L}^{JS}(\mathbf{q}', \mathbf{q})$. Therefore the Lorentz invariant amplitudes $F_m^I(|\mathbf{q}|, \theta)$ and $g_m^I(|\mathbf{q}|, \theta)$, Eqs. (29) and (32), as well as the transformation matrix C_{im} of Eq. (31) depend on $\tilde{M}^*$ and the Fermi momentum k_F because the plane-wave helicity states $|\lambda_1\lambda_2 \mathbf{q}\rangle$ of Eq. (30) are now medium dependent (58). The next step is to compute the self-energy components Σ_s, Σ_0, and $\mathbf{k}\Sigma_v$. Because the Dirac propagator (36) describes dressed quasi particles now, in Eqs. (41), (42), and (43) the mass M and energy E have to be replaced by the effective quantities $\tilde{M}^*$, $\tilde{E}^*$. Finally the new $\tilde{M}^*$ is determined. This iteration procedure is repeated until convergence is reached.

In Fig. 12 the results for the self-consistently calculated self-energy components Σ_s and Σ_0 for Bonn A, Nijm 93, and Nijmegen I are shown as a function of the Fermi momentum and compared to the tree-level results from Fig. 6. For the Bonn A case the result of a full self-consistent DBHF calculation is shown as well [14]. From this figure two features can be observed: the higher-order density dependences that are introduced by the dressing of the potential affect mainly the scalar part of the self-energy. The modifications of Σ_0 are moderate, whereas Σ_s is significantly reduced. The short-range ladder correlations included in the full DBHF calculation (Bonn A) influence the self-energy in an opposite way. The deviations of Σ_s from the self-consistent HF result are rather small, however, the vector component gets now strongly suppressed. This fact is understandable because the ladder correlations prevent the two-nucleon wave functions from overlapping too strongly with the hard core. In OBE potentials the hard core is mainly mediated by vector ω exchange and thus determines the vector self-energy component.

With the self-consistent Hartree-Fock self-energies at hand one can now determine the equation of state (EOS). As in DBHF the EOS, i.e., the energy per particle, is defined as the
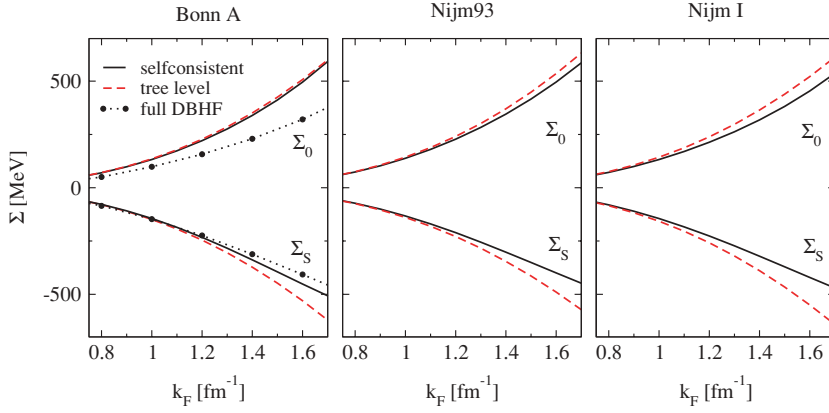
FIG. 12. (Color online) Comparison of the tree-level scalar and vector self-energy components (dashed line) with self-consistent results (solid line). Additionally a full self-consistent DBHF calculation is shown in the first graph denoted by dots.

kinetic plus half of the potential energy

$$E/A = \frac{1}{\rho} \sum_{\mathbf{k},\lambda} \langle \overline{u}_\lambda^*(\mathbf{k}) | \boldsymbol{\gamma} \cdot \mathbf{k} + M + \frac{1}{2}\Sigma(k) | u_\lambda^*(\mathbf{k}) \rangle \frac{\tilde{M}^*}{\tilde{E}^*} - M \tag{60}$$

$$= \frac{1}{\rho} \int_F \frac{d^3\mathbf{k}}{2\pi^3} \left\{ [1 + \Sigma_v(|\mathbf{k}|)]\tilde{E}^* - \Sigma^0(|\mathbf{k}|) \right.$$
$$\left. - \frac{1}{2\tilde{E}^*} [\Sigma_s(|\mathbf{k}|)\tilde{M}^* - \Sigma_\mu(|\mathbf{k}|)\tilde{k}^{*\mu}] \right\} - M \tag{61}$$

with the self-consistent spinors u_λ^* from Eq. (58).

In Fig. 13, we present the self-consistent Hartree-Fock results for the energy per particle in symmetric nuclear matter calculated from the Bonn A, Nijm93, Nijmegen I potentials as a function of the Fermi momentum k_F, which is a measure for the density $\rho = 2/(3\pi^2)k_F^3$.

Also a non-self-consistent calculation is shown (dashed line) where the energy per particle is given by

$$E/A = \frac{1}{\rho} \int_F \frac{d^3\mathbf{k}}{2\pi^3} \left[\frac{k^2}{2M} + \frac{1}{2} U_{\text{s.p.}}(k, k_F) \right], \tag{62}$$

with $U_{\text{s.p.}}(k, k_F)$ as defined in Eq. (45). In this case one obtains the same result as in a nonrelativistic Hartree-Fock calculation (denoted by stars in Fig. 13). The latter demonstrates again the numerical accuracy of the procedures.

For the Bonn A case again the equation of state from the full DBHF calculations is shown as a Ref. [14]. It is clear that ladder correlations and other in-medium effects such as Pauli blocking of intermediate states in the Bethe-Salpeter equation are responsible for nuclear saturation. The relatively moderate deviations from self-consistent Hartree-Fock at the scale of the self-energies in Fig. 12 are essential at the scale of the binding energy. Like in relativistic mean-field theory of QHD subtle cancelation effects in the large scalar and vector fields are responsible for nuclear binding.

The higher-order density dependences introduced via the dressing of the bare interaction V lead to significantly more repulsion at the level of the equation of state. This is a direct consequence of the reduced attractive scalar field (see Fig. 12). Thus Fig. 13 serves also as a demonstration for the success of DBHF compared to BHF what concerns the quantitative description of nuclear saturation: In particular for modern high-precision potentials such as Bonn, Nijmegen, or Argonne v_{18} the BHF approach leads to strong over-binding and too high saturation densities. The additional repulsion introduced by higher-order terms in density through the dressed potentials shifts the corresponding saturation points toward the empirical region [13,16,55]. We want to stress that the density dependence of the dressed potential V^* should not be mixed up with the density dependence of the G matrix. The latter originates from the dressed two-nucleon propagator and the Pauli operator in the Bethe-Goldstone (or Bethe-Salpeter) equations, whereas V^* enters into the Bethe-Salpeter for
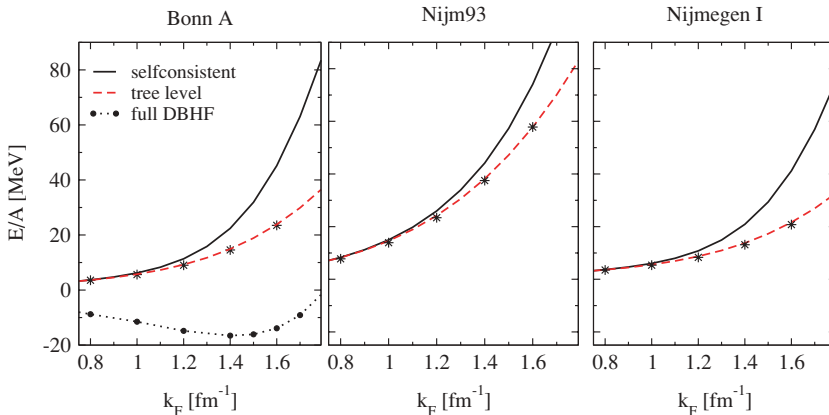

FIG. 13. (Color online) Hartree-Fock calculation of the nuclear equation of state, i.e., energy per particle E/A as a function of the Fermi momentum k_F for three different potentials. The dashed line indicates a tree-level calculation and the solid line represents a self-consistent Hartree-Fock calculation, i.e., higher-order corrections in density are included.

iteration. In non-relativistic BHF or variational calculations [56,57] a nonlinear density dependence that improves the saturation behavior is usually introduced through net repulsive three-body forces. In such a treatment the dependence on the third particle is integrated out such that one is left with an additional effective density-dependent two-body force that acts in a similar way as a dressing of the two-body interaction. In this context one should mention that a dressing of the interaction has also more subtle consequences when iterated in the Bethe-Salpeter equation. It leads, e.g., to a quenching of the second-order OPE exchange [58] that plays an essential role for saturation in nonrelativistic approaches.

In summary, one could expect that a dressing of the interaction would allow to comply with weaker three-body forces which may in particular be of interest concerning the application of low momentum EFT potentials to the nuclear many-body problem. As the studies of Bogner *et al.* [51] have demonstrated, $V_{\text{low }k}$ requires rather strong three-body forces to stabilize nuclear matter. There the strength of the three-body contributions has already been pushed to its limits. Although a dressing of the interaction will probably not be possible for $V_{\text{low }k}$ due to the partially nonanalytic structure of the potential, it may be a promising perspective for the application of other EFT potentials, e.g., the chiral N^{3}LO.

VII. SUMMARY

The appearance of large scalar and vector fields is a well-established feature of relativistic nuclear dynamics. The saturation mechanism of nuclear matter or the single particle potential in finite nuclei are obtained by subtle cancelation effects between large attractive scalar and repulsive vector fields. These fields occur already at tree level and do not change too much when realistic many-body calculations are performed. Full self-consistent Brueckner calculations that account for short-range ladder correlations lead to mean fields of similar size, i.e., of several hundred MeV in magnitude. The size of the scalar-vector fields coincides with the values derived from relativistic mean-field phenomenology by fits to finite nuclei. Alternatively, QCD sum rules come to the same results.

The present work addresses the question about the origin of these fields. When the nucleon-nucleon interaction is described within the framework of a meson exchange picture, the situation is rather clear. The Lorentz character of the mesons determines automatically the Lorentz character of the interaction at the corresponding scale: the short-range repulsion is due to vector exchange (ω, ρ), whereas the intermediate range attraction originates from scalar exchange (σ). As a direct consequence this leads to the existence of large scalar and vector mean fields in nuclear matter. However, these fields are not observables. It is therefore a fundamental questions of nuclear physics whether the appearance of large scalar/vector fields is intimately connected to the meson-exchange picture or if it is a general consequence of the vacuum *NN* interaction.

To address the question in a model-independent way, we based the present study on a broad set of modern high-precision *NN* potentials: Bonn, CD-Bonn, Nijmegen, Argonne v_{18}, Reid93, Idaho N^{3}LO, and $V_{\text{low }k}$. Except the fact that all

these potentials fit *NN*-scattering data with high accuracy they are based partially on quite different theoretical concepts, i.e., the traditional meson-exchange picture (Bonn, CD-Bonn, Nijmegen), a purely phenomenological philosophy (Argonne v_{18}, Reid93) or QCD-inspired EFT approaches (Idaho N^{3}LO, $V_{\text{low }k}$).

For this purpose the potentials were projected on a relativistic operator basis in Dirac space. This was achieved using standard projection techniques that transform from a partial wave basis, i.e., the basis where the potentials are originally given, to the basis of covariant amplitudes in Dirac space. The idea behind this approach is that both relativistic and nonrelativistic descriptions of the *NN* interaction have common features, i.e., they are based on a certain operator structure in spin-isospin space and invoke certain scales: the long-range part of scale m_π, essentially given by one-pion exchange, the intermediate range attraction and the short-range repulsion. In the meson exchange picture the various scales are associated with the meson masses that mediate the interaction. The various approaches can now be compared at the level of these covariant amplitudes where we observe a remarkable agreement between the meson exchange potentials (Bonn, CD-Bonn, Nijmegen), the phenomenological nonrelativistic potentials (Argonne v_{18}, Reid93), and the EFT potentials (Idaho N^{3}LO, $V_{\text{low }k}$).

Moreover, this procedure now allows the calculation of the relativistic self-energy operator in nuclear matter. The key result of the present investigations is the tree-level self-energy in nuclear matter. The structure of the nucleon-nucleon interaction enforces the existence of large scalar and vector fields. This is found to be a model-independent fact, true for all types of interactions that have been considered. The scale of these fields is set at tree level. Although essential for nuclear binding and saturation, higher-order correlations, in particular short-range correlations, change the size of the fields by less than 25%. The magnitude of the tree-level fields is very similar to that predicted by relativistic mean-field phenomenology and relativistic many-body calculations.

The connection to QCD as the underlying theory of strong interactions is established by chiral effective theory. EFT nucleon-nucleon potentials are derived from a systematic expansion of an effective Lagrangian that respects the basic symmetries of QCD. Chiral EFT is considered as the exact mapping of QCD on effective hadronic degrees of freedom in the nonperturbative regime. Subjecting the chiral N^{3}LO Idaho potential to the present projection scheme we can make the following statements: In nuclear matter scalar and vector mean fields of the same sign and magnitude are generated as by the meson exchange or phenomenological potentials. These fields are generated by contact terms that occur at next-to-leading order in the chiral expansion. These are four-nucleon contact terms with two derivatives that generate the short-range spin-orbit interaction. The strength of the corresponding low energy constants, in particular those connected to the spin-orbit force, is dictated by *P*-wave *NN*-scattering data. Pion dynamics as well as LO and N^{3}LO contacts provide only corrections to the fields generated by the NLO contact terms. EFT is therefore in perfect agreement with Dirac phenomenology where it has long been known that the large scalar/vector fields are

generated by the short-range vector (ω) and scalar (σ) mesons that are connected intimately to the large spin-orbit interaction. We conclude that this is a direct consequence of P-wave NN scattering.

As in OBE models and RMF theory, in EFT the reduction of the nucleon mass $M^* = M + \Sigma_s$ is driven by short-distance physics. Long-distance physics from virtual pions, i.e., the nonanalytic term in the expansion of σ_N, gives a sizable contribution to the modification of the in-medium quark condensate. Such contributions are, however, found to play only a minor role for the reduction of the nucleon mass. Nevertheless, at moderate nuclear densities the N^{3}LO scalar and vector fields agree almost perfectly with the prediction from leading-order QCD sum rules. For future perspectives chiral EFT in combination with projection techniques may allow a determination of the relativistic antiproton potential in matter in a model-independent way. Here the meson-exchange picture predicts a change in sign of the vector field due to g parity and hence an extremely deep attractive potential. Such investigations in particular will be interesting in view of the forthcoming antiproton facilities, e.g., Panda at FAIR [59].

Finally we investigated implications of higher-order corrections in density on the nuclear equation of state. A dressing of the potential through self-consistently determined self-energies leads to significantly more repulsion in the equation of state as early as the Hartree-Fock level. At present these investigations were restricted to OBE-type potentials. But to include such higher-order terms in density might open a promising perspective also for EFT potentials when applied to the nuclear many-body problem.

[1] B. D. Serot and J. D. Walecka, *Advances in Nuclear Physics*, edited by J. W. Negele and E. Vogt (Plenum, New York, 1986), Vol. 16, p. 1.

[2] P. Ring, Prog. Part. Nucl. Phys. **37**, 193 (1996); Lect. Notes Phys. **641**, 175 (2004).

[3] A. Arima, M. Harvey, and K. Shimizu, Phys. Lett. **B30**, 517 (1969).

[4] J. N. Ginocchio, Phys. Rev. Lett. **78**, 436 (1997).

[5] A. V. Afanasjev, J. König, and P. Ring, Phys. Lett. **B367**, 11 (1996).

[6] T. D. Cohen, R. J. Furnstahl, and D. K. Griegel, Phys. Rev. Lett. **67**, 961 (1991); Phys. Rev. C **45**, 1881 (1992).

[7] E. G. Drukarev and E. M. Levin, Prog. Part. Nucl. Phys. **27**, 77 (1991).

[8] B. L. Ioffe, Nucl. Phys. **B188**, 317 (1981).

[9] P. Finelli, N. Kaiser, D. Vretenar, and W. Weise, Eur. Phys. J. A **17**, 573 (2003); Nucl. Phys. **A735**, 449 (2004).

[10] K. A. Brueckner and J. L. Gammel, Phys. Rev. **107**, 1023 (1958).

[11] M. R. Anastasio, L. S. Celenza, W. S. Pong, and C. M. Shakin, Phys. Rep. **100**, 327 (1983).

[12] B. ter Haar and R. Malfliet, Phys. Rep. **149**, 207 (1987).

[13] R. Brockmann and R. Machleidt, Phys. Rev. C **42**, 1965 (1990).

[14] T. Gross-Boelting, C. Fuchs, and Amand Faessler, Nucl. Phys. **A648**, 105 (1999).

[15] E. van Dalen, C. Fuchs, and A. Faessler, Nucl. Phys. **A744**, 227 (2004); E. N. E. van Dalen, C. Fuchs, and A. Faessler, Phys. Rev. Lett. **95**, 022302 (2005); Phys. Rev. C **72**, 065803 (2005).

[16] C. Fuchs, Lect. Notes Phys. **641**, 119 (2004).

[17] R. Machleidt, K. Holinde, and Ch. Elster, Phys. Rep. **149**, 1 (1987).

[18] R. B. Wiringa, V. G. J. Stoks, and R. Schiavilla, Phys. Rev. C **51**, 38 (1995).

[19] V. G. J. Stoks, R. A. M. Klomp, C. P. F. Terheggen, and J. J. de Swart, Phys. Rev. C **49**, 2950 (1994).

[20] V. G. J. Stoks, R. A. M. Klomp, M. C. M. Rentmeester, and J. J. de Swart, Phys. Rev. C **48**, 792 (1993).

[21] M. M. Nagels, T. A. Rijken, and J. J. de Swart, Phys. Rev. D **17**, 768 (1978).

[22] D. R. Entem and R. Machleidt, Phys. Rev. C **66**, 014002 (2002).

[23] D. R. Entem and R. Machleidt, Phys. Rev. C **68**, 041001(R) (2003).

[24] E. Epelbaum, W. Glöckle, and U.-G. Meissner, Nucl. Phys. **A747**, 362 (2005).

[25] S. K. Bogner, T. T. S. Kuo, and A. Schwenk, Phys. Rep. **386**, 1 (2003).

[26] J. A. Tjon and S. J. Wallace, Phys. Rev. C **32**, 267 (1985).

[27] C. J. Horowitz and B. D. Serot, Nucl. Phys. **A464**, 613 (1987).

[28] R. Machleidt, Phys. Rev. C **63**, 024001 (2001).

[29] R. Machleidt and I. Slaus, J. Phys. G **27**, R69 (2001).

[30] H. Müther and A. Polls, Prog. Part. Nucl. Phys. **45**, 243 (2000).

[31] R. Machleidt, in: *Computational Nuclear Physics 2—Nuclear Reactions*, edited by K. Langanke, J. A. Maruhn, and S. E. Koonin (Springer, New York, 1993), Chap. 1, p. 1.

[32] S. Weinberg, Phys. Lett. **B251**, 288 (1990); Nucl. Phys. **B363**, 3 (1991).

[33] N. Kaiser, Phys. Rev. C **63**, 044010 (2001); **64**, 057001 (2001); **65**, 017001 (2002).

[34] J. A. Tjon and S. J. Wallace, Phys. Rev. C **32**, 1667 (1985).

[35] C. Fuchs, T. Waindzoch, A. Faessler, and D. S. Kosov, Phys. Rev. C **58**, 2022 (1998).

[36] K. Erkelenz, Phys. Rep. **13**, 191 (1974).

[37] R. Machleidt, Adv. Nucl. Phys. **19**, 189 (1989).

[38] M. Rose, *Elementary Theory of Angular Momentum* (Wiley, New York, 1957).

[39] L. Sehn, C. Fuchs, and A. Faessler, Phys. Rev. C **56**, 216 (1997).

[40] This code was provided by H. Müther and used in the Born option. For each potential partial waves up to $J = 9$ are taken into account.

[41] M. C. Birse, Phys. Rev. C **53**, R2048 (1996).

[42] G. Chanfray, M. Ericson, P. A. M. Guichon, Phys. Rev. C **63** 055202 (2001).

[43] J. Gasser and H. Leutwyler, Phys. Rep. **87**, 77 (1982).

[44] This investigation is based on a version of the chiral N^{3}LO Idaho potential which allows to seperate the contributions from different orders. The code was provided by R. Machleidt (private communication).

[45] R. Thomas, S. Zschocke, and B. Kämpfer, Phys. Rev. Lett. **95**, 232301 (2005).

[46] O. Plohl, C. Fuchs, and E. N. E. van Dalen, Phys. Rev. C **73**, 014003 (2006).

[47] E. Schiller and H. Müther, Eur. Phys. J. A **11**, 15 (2001).

[48] T. Becher and H. Leutwyler, Eur. Phys. J. C **9**, 643 (1999).

[49] T. Becher and H. Leutwyler, J. High Energy Phys. 06 (2001) 017.

[50] J. Kuckei, F. Montani, H. Müther, and A. Sedrakian, Nucl. Phys. **A723**, 32 (2003).

[51] S. K. Bogner, A. Schwenk, R. J. Furnstahl, and A. Nogga, Nucl. Phys. **A763**, 59 (2005).

[52] N. Kaiser, Phys. Rev. C **70**, 034307 (2004).

[53] P.-G. Reinhard and M. Bender, Lect. Notes Phys. **641**, 249 (2004).

[54] B. Cochet, K. Bennaceur, J. Meyer, P. Bonche, and T. Duguet, Int. J. Mod. Phys. E **13**, 187 (2004).

[55] C. Fuchs and H. H. Wolter, nucl-th/0511070, to appear in Eur. Phys. J. A.

[56] X. R. Zhou, G. F. Burgio, U. Lombardo, H.-J. Schulze, and W. Zuo, Phys. Rev. C **69**, 018801 (2004).

[57] A. Akmal, V. R. Pandharipande, and D. G. Ravenhall, Phys. Rev. C **58**, 1804 (1998).

[58] M. K. Banerjee and J. A. Tjon, Phys. Rev. C **58**, 2120 (1998); Nucl. Phys. **A708**, 303 (2002).

[59] K. Peters, Nucl. Phys. B (Proc. Suppl.) **154**, 35 (2006).